DTIC® has determined on *14/05/2009* that this Technical Document has the Distribution Statement checked below. The current distribution for this document can be found in the DTIC® Technical Report Database.

☒ **DISTRIBUTION STATEMENT A.** Approved for public release; distribution is unlimited.

☐ **© COPYRIGHTED**; U.S. Government or Federal Rights License. All other rights and uses except those permitted by copyright law are reserved by the copyright owner.

☐ **DISTRIBUTION STATEMENT B.** Distribution authorized to U.S. Government agencies only (fill in reason) (date of determination). Other requests for this document shall be referred to (insert controlling DoD office)

☐ **DISTRIBUTION STATEMENT C.** Distribution authorized to U.S. Government Agencies and their contractors (fill in reason) (date of determination). Other requests for this document shall be referred to (insert controlling DoD office)

☐ **DISTRIBUTION STATEMENT D.** Distribution authorized to the Department of Defense and U.S. DoD contractors only (fill in reason) (date of determination). Other requests shall be referred to (insert controlling DoD office).

☐ **DISTRIBUTION STATEMENT E.** Distribution authorized to DoD Components only (fill in reason) (date of determination). Other requests shall be referred to (insert controlling DoD office).

☐ **DISTRIBUTION STATEMENT F.** Further dissemination only as directed by (inserting controlling DoD office) (date of determination) or higher DoD authority.

Distribution Statement F is also used when a document does not contain a distribution statement and no distribution statement can be determined.

☐ **DISTRIBUTION STATEMENT X.** Distribution authorized to U.S. Government Agencies and private individuals or enterprises eligible to obtain export-controlled technical data in accordance with DoDD 5230.25; (date of determination). DoD Controlling Office is (insert controlling DoD office).

REPORT DOCUMENTATION PAGE

The public reporting burden for this collection of information is estimated to average 1 hour per response, including the time for reviewing instructions, searching existing data sources, gathering and maintaining the data needed, and completing and reviewing the collection of information. Send comments regarding this burden estimate or any other aspect of this collection of information, including suggestions for reducing the burden, to the Department of Defense, Executive Service Directorate (0704-0188). Respondents should be aware that notwithstanding any other provision of law, no person shall be subject to any penalty for failing to comply with a collection of information if it does not display a currently valid OMB control number.
PLEASE DO NOT RETURN YOUR FORM TO THE ABOVE ORGANIZATION.

1. REPORT DATE (DD-MM-YYYY)	2. REPORT TYPE		3. DATES COVERED (From - To)
06/03/2009	Final		2/15/06-2/15/09

4. TITLE AND SUBTITLE	5a. CONTRACT NUMBER
INTERFACE CONDITIONS FOR HYBRID RANS/LES SIMULATIONS OF COMPLEX AND COMPRESSIBLE FLOWS	
	5b. GRANT NUMBER
	FA9550-06-1-0116
	5c. PROGRAM ELEMENT NUMBER
6. AUTHOR(S)	5d. PROJECT NUMBER
Ugo Piomelli and Elias Balaras	
	5e. TASK NUMBER
	5f. WORK UNIT NUMBER

7. PERFORMING ORGANIZATION NAME(S) AND ADDRESS(ES)	8. PERFORMING ORGANIZATION REPORT NUMBER
University of Maryland Department of Mechanical Engineering College Park, MD 20742	

9. SPONSORING/MONITORING AGENCY NAME(S) AND ADDRESS(ES)	10. SPONSOR/MONITOR'S ACRONYM(S)
Air Force Office of Scientific Research /NA 875 North Randolph Street Suite 325, Rm 3112 Arlington, VA 22203 Dr. John Schmisseur	AFOSR
	11. SPONSOR/MONITOR'S REPORT NUMBER(S)

12. DISTRIBUTION/AVAILABILITY STATEMENT
Public

13. SUPPLEMENTARY NOTES

14. ABSTRACT
We have demonstrated the applicability of synthetic turbulence coupled with the controlled-forcing method to generate eddies at the interface between RANS and LES in hybrid calculations. We obtained shorter transition regions and improved model accuracy. Realistic turbulence can be generated within 5 boundary-layer thicknesses of the RANS/LES interface even in cases in which the data supplied by the RANS is inaccurate, or the assumptions on which the forcing is based are invalid. We applied this technique in a variety of turbulent flows with uniformly good results. A single-block hybrid calculation was performed in a geometry that, although simple, presented several difficulties. We demonstrated that unless turbulent eddies are artificially generated at the RANS/LES interface, very significant errors appear in the flow statistics even at low order (skin-friction coefficient, mean velocity profile). Establishing realistic turbulent eddies capable to transport momentum, energy and mass, appears to be a critical factor for the accurate prediction of shallow separation by hybrid RANS/LES methods.

15. SUBJECT TERMS

16. SECURITY CLASSIFICATION OF:			17. LIMITATION OF ABSTRACT	18. NUMBER OF PAGES	19a. NAME OF RESPONSIBLE PERSON
a. REPORT	b. ABSTRACT	c. THIS PAGE			
				29	19b. TELEPHONE NUMBER (Include area code)

Final Report

Grant No. FA9550-06-1-0116

INTERFACE CONDITIONS FOR HYBRID RANS/LES SIMULATIONS OF COMPLEX AND COMPRESSIBLE FLOWS

Objectives

To develop efficient and robust ways to match solutions of the Reynolds-Averaged Navier-Stokes equations to the large-eddy simulation. These methods will be tested in flows with pressure-driven and unsteady separation and in three-dimensional boundary layers.

Summary of results

We have demonstrated the applicability of synthetic turbulence coupled with the controlled-forcing method to generate eddies at the interface between RANS and LES in hybrid calculations. By investigating the effects of the model parameter, and developing guidelines to set their values, we obtained shorter transition regions and improved model accuracy. It was found that realistic turbulence (with the correct statistics) can be generated within 5 boundary-layer thicknesses of the RANS/LES interface even in cases (such as the accelerating boundary layer) in which the data supplied by the RANS is inaccurate, or the assumptions on which the forcing is based are invalid.

We applied this technique in a variety of turbulent flows including phenomena such as freestream acceleration, separation, and mean flow three-dimensionality, with uniformly good results. A single-block hybrid calculation was then performed in a geometry that, although simple, presented several difficulties: because of the shallow pressure-driven separation, incorrect prediction of the upstream flow results in significant errors that propagate downstream, as the shear layer instability acts as an error amplifier. We demonstrated that unless turbulent eddies are artificially generated at the RANS/LES interface, very significant errors appear in the flow statistics even at low order (skin-friction coefficient, mean velocity profile). Establishing realistic turbulent eddies capable to transport momentum, energy and mass, appears to be a critical factor for the accurate prediction of shallow separation by hybrid RANS/LES methods.

20090429203

1

Accomplishments

1 Introduction

1.1 Motivation

Recent years have seen the increased availability of inexpensive parallel computer clusters able to reduce the computational time for the solution of numerical models. This development has allowed to extend the numerical solution of the Navier-Stokes equations to turbulent flows in more realistic configurations than possible until now.

Turbulent flows can be studied by direct numerical simulations (DNS) of the Navier Stokes equation, in which the grid resolution is sufficient to resolve all the scales of motion. This method constitutes the conceptually simplest approach to the problem of turbulence. Practically, however, the cost of DNS confines this method to low-Reynolds-number applications: Assuming that computer power will increase by a factor of five every five years, Spalart [36] estimated that DNS will not be applicable to the flow over an airliner or a car until 2080.

In large-eddy simulations (LES) the target is to simulate only the eddies containing the bulk of the energy of the flow, while modeling the dissipative scales. These scales are generally anisotropic and dependent on the boundary conditions (therefore, extremely difficult to model); the fact that the small eddies are modeled reduces the cost of LES considerably compared with DNS, especially in free shear flows. However, when LES are applied to wall-bounded flows at high Reynolds numbers, the number of grid points required to resolve the energy-carrying eddies is proportional to $Re^{1.8}$, which again makes this technique only suitable for moderate Reynolds-number applications. Wall-Modeled LES (WMLES), in which the inner layer is modeled either by the Reynolds-Averaged Navier-Stokes (RANS) equations or through approximate boundary conditions, may alleviate this problem (see the review in [22]). Spalart [36], however, estimates that even the application of WMLES to external flow of aeronautical interest is several decades away for external aerodynamics (in environmental or oceanographic flows, in which the Reynolds numbers are comparably high, but the boundary layers are thicker, WMLES is already applicable to practical problems).

Traditionally, high-Reynolds-number flows have been predicted using the Reynolds-Averaged Navier-Stokes (RANS) equations. RANS model are designed to be accurate in a variety of design flows (such as thin shear layers) but lose accuracy in the presence of fluid-dynamical non-equilibrium (transition or re-laminarization, strong streamline curvature, strong flow acceleration or deceleration). A possible avenue to solve practical engineering flows, then, is by using a combination of RANS and LES, in which the RANS equations are solved in quasi-equilibrium regions or where they can be accurately tuned, while LES or WM-LES are used in non-equilibrium regions, where the RANS models are expected to fail. Hybrid RANS/LES techniques have emerged as a tool that allows the simulation of complex fluid flows within reasonable amounts of CPU time.

One issue that arises when hybrid RANS/LES methods are used is the behavior of the flow in the transition zone between the RANS and LES regions and how that region affects the results downstream. In the RANS zone the flow solution is either steady, or only contains information on the largest scales of motion if mean-flow unsteadiness is present; most (or all) of the Reynolds shear stress is provided by the turbulence model. In the LES region, on the other hand, the resolved scales must supply most of the Reynolds shear stress, and eddies must be present to provide it. Typically, a transition zone exists in which resolved eddies are generated gradually and grow; in this region the flow may be unphysical. Different techniques to trigger the instabilities have been developed.

One of the most popular hybrid RANS/LES techniques is the Detached Eddy Simulation [38] (DES). In this model the switch between RANS and LES is determined by the grid size: when the mesh becomes small enough to resolve the energy-carrying eddies the eddy viscosity is reduced. Modifications of this model to link the RANS/LES transition to the turbulent viscosity, thus avoiding premature switch from the RANS to the LES region have also been proposed and show potential [35]. In standard applications of this method (Figure 1), the thin attached shear layers are modeled by RANS, and only away from solid bodies the technique switches to LES, and the RANS/LES interface occurs generally in the separated shear layers,
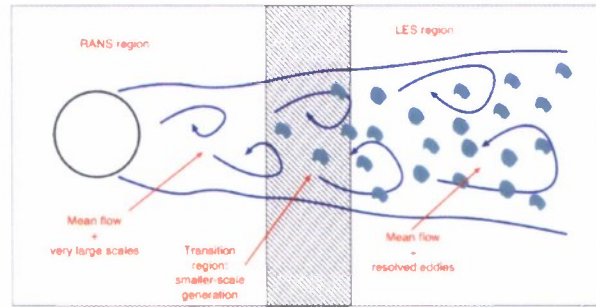
Figure 1: Sketch of the interface region between RANS and LES regions in a massively separated flow.

where the strong instability caused by the inflection points in the velocity profiles is extremely beneficial for the generation of energy-carrying eddies: any disturbance present in the flow is quickly amplified, resulting in a very short transition region. However, an important future field of application for hybrid method is in aeronautical applications such as that sketched in Figure 2, in which attached boundary layers are computed using the RANS approach, while LES is used in the separated flow regions. The application of DES to flows with weaker instability mechanisms may create problems: if the turbulent eddies do not grow sufficiently fast, the simulations can become inaccurate, as the modeled shear stress decreases while the resolved one does not increase sufficiently fast. Such quantities as the mean velocity profile, skin friction coefficient and separation location can be in error. In fact, when DES is used as a wall-layer model [20], no such instabilities exist, and a significant transition region is observed between the smooth inner layer (in which RANS equations are solved) and the outer LES region, in which turbulent eddies are gradually formed (see the discussion in [22]). This transition region results in a displacement of the logarithmic layer and errors in the prediction of the skin-friction coefficient in the plate.

Under a previous Grant, the PIs investigated the generation of inflow conditions for large-eddy simulations. The methodology developed can be used for hybrid RANS/LES models in which two separate calculations are carried out: with reference to Figure 2, a RANS solution of the entire domain is first performed, which supplies the boundary conditions for the LES region. The present grant aims to optimize this method, and use it in actual hybrid calculations, stressing flows with pressure-driven or unsteady separation (as opposed to the massively separated flows to which DES has been applied successfully). In these configurations, the accurate prediction of the momentum transport due to the resolved eddies is critical; as we shall show, the absence of turbulent eddies at the RANS/LES interface may lead to significant inaccuracies in the prediction of the separation point, and of the flow downstream in the recovery region.
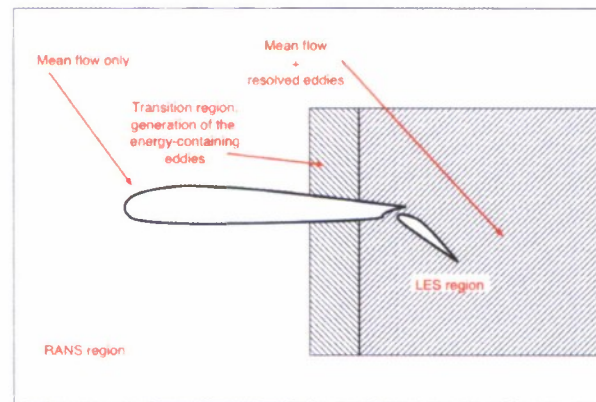

Figure 2: Sketch of the interface region between RANS and LES regions for an aerodynamic application.

3

1.2 Organization of this report

This report is organized as follow: we begin by summarizing the forcing method that had been developed during the previous grant cycle. We will then discuss the optimization of the model parameters. Finally, we will present the results of actual hybrid calculations of the flow over a contoured ramp.

2 Turbulence generation techniques

2.1 Review of existing methods

We focus on a class of applications, of the type shown in Figure 2, in which RANS is used in equilibrium regions of the flow, while LES is performed in a small part of the domain, possibly including attached boundary layers as well as separated flow. In this configuration the generation of energy- and momentum-carrying eddies can be expected to be slow, as the instability mechanism in the attached boundary layer is weaker than in the separated shear layers that dominate the dynamics of massively separated flows. It is the purpose of this work to investigate methods to speed up the development of such turbulent structures, to obtain a realistic distribution of eddies in the shortest possible length for different fluid flow problems.

Reviews of turbulence generation methods for problems of this type can be found in [9, 6], among other places. Here, we summarize the main issues involved. Two methods can be used to perform hybrid calculations: the RANS and LES zones can be computed separately, with the RANS information used to assign the inflow boundary condition for the LES; or, a single calculation can be carried out (as in DES) in which the model switches from RANS to LES. The simplest method to generate turbulence at an interface between a RANS and an LES zone, if separate calculations are used, is by prescribing a mean flow to which velocity fluctuations that meet certain criteria are superposed. If a single calculation is performed, the same result can be achieved by including a forcing term in the equations that generates the desired random perturbations.

Random fluctuations with given moments and spectra have been used, for example, in [13, 12]. Since the fluctuations lack phase information, however, the turbulence levels decays rapidly, and only some distance downstream of the inflow plane (or of the RANS/LES interface) the turbulent eddies are regenerated. More advanced methods that attempt to reproduce the eddy structure of a wall-bounded flow at the inflow have been proposed [32, 26, 11, 1, 3, 16]. They achieve improved results (compared with the simple superposition of random fluctuations) by a judicious assignment of the turbulence spectrum and by trying to match the flow anisotropy. Since none of these method contains realistic phase information between the modes, an adjustment region downstream of the inflow is unavoidable. In this region the initial fluctuations are selectively amplified or dissipated by the flow, and realistic turbulent eddies are generated.

This was shown by Keating *et al.* [9], who compared various types of inflow conditions for LES, among them the use of random noise, the adapted database method by Schlüter [27], the synthetic turbulence generation method proposed by Batten *et al.* [1], and a technique based on controlled forcing proposed by Spille-Kohoff and Kaltenbach [39]. The latter method is based on the selective amplification of strong bursts downstream of an inflow supplied by a synthetic turbulence generation method. A controller is used at several location downstream of the inflow to determine the amplitude of a forcing term in the wall-normal momentum equation. This term reinforces the more realistic eddies, by requiring that a target Reynolds shear-stress profile (obtained from the RANS, or from experiments) be achieved. Keating *et al.* [9] found that the adapted-database and the controlled-forcing methods resulted in significantly shorter development lengths than any of the other techniques. Later, Keating *et al.* [6] applied the controlled-forcing method in a hybrid RANS/LES framework for the simulation of boundary layers in favorable and adverse pressure gradients, and again found that it produced physically realistic turbulence in short distances. They also observed that the quality of the RANS data used affects the results significantly; this is true in particular in favorable and adverse-pressure-gradient boundary layers.

In the following we will first describe the methodology used, then discuss the controller function, and the optimization of its parameters. The result of its application will be presented next.
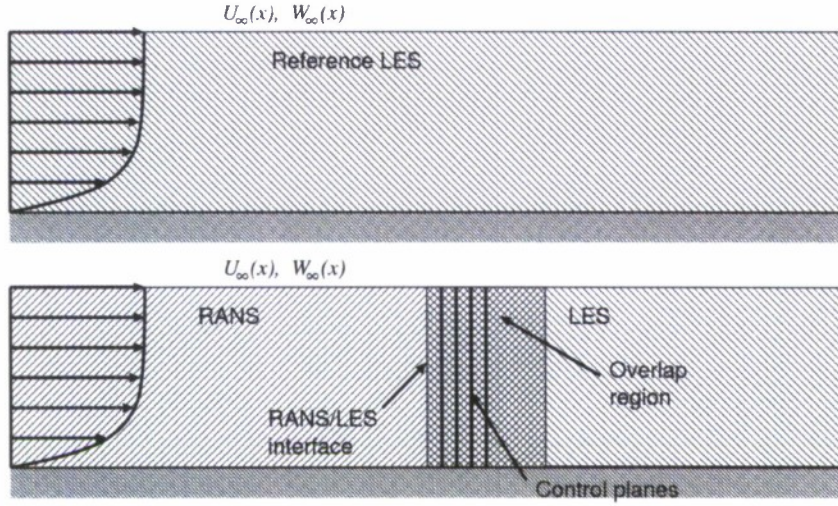
Figure 3: Sketch of the geometric configuration.

2.2 Methodology

2.2.1 Problem setup

As mentioned above, hybrid methods can be developed both for a single grid (as in the DES applications [38]), or using separate grids in the separate zones. This last approach allows, if desired, to decouple the RANS calculation from the LES one (as is the case in the study of the flow in a turbine by Schlüter *et al.* [28]). For the purposes of testing eddy-generation methods, the latter approach is the most economical, since the RANS is performed only once, and its results can be used both to supply the inflow conditions, and also to control the forcing. We will, therefore, follow this methodology. The tests described will all be performed using the same strategy as [9, 6] (see Figure 3): first we perform a reference LES of the entire domain of interest; then we perform a RANS calculation of the equilibrium region, and use the RANS statistics to assign the inflow of the LES. Comparisons between the hybrid RANS/LES and the reference calculation allow us to evaluate the effectiveness of the method.

2.2.2 Governing equations and numerical method

In LES the velocity field is separated into a resolved (large-scale) and a subgrid (small-scale) field, by a spatial filtering operation. In the unsteady RANS (URANS) approach, on the other hand, the Reynolds decomposition is used to separate the mean from the fluctuating part of the velocity. Despite this difference, the governing equations for LES and URANS have the same form:

$$\frac{\partial \overline{u}_i}{\partial x_i} = 0, \tag{1}$$

$$\frac{\partial \overline{u}_i}{\partial t} + \frac{\partial (\overline{u}_j \overline{u}_i)}{\partial x_j} = \nu \frac{\partial^2 \overline{u}_i}{\partial x_j \partial x_j} - \frac{\partial \tau_{ij}}{\partial x_j} - \frac{1}{\rho} \frac{\partial \overline{p}}{\partial x_i}. \tag{2}$$

In these equations, an overline denotes a quantity averaged over one grid cell and time step, and $\tau_{ij} = \overline{u_i u_j} - \overline{u}_i \overline{u}_j$ are either the subgrid-scale (SGS) stresses or the Reynolds stresses that must be modeled. In both regions an eddy-viscosity model is used to close the above set of equations:

$$\tau_{ij} - \frac{\delta_{ij}}{3} \tau_{kk} = -2\nu_t \overline{S}_{ij}. \tag{3}$$

The model used in the LES region to parameterize the SGS stresses is the Lagrangian dynamic eddy-viscosity model [5, 17]. In the RANS region the Spalart-Allmaras (SA) one-equation model [34] is used. The model

5

solves a transport equation for an auxiliary variable $\widetilde{\nu}$:

$$\frac{D\widetilde{\nu}}{Dt} = c_{b1}\widetilde{S}\widetilde{\nu} - c_{w1}f_w \left[\frac{\widetilde{\nu}}{\widetilde{d}}\right]^2 + \frac{1}{\sigma}\left\{\nabla \cdot \left[(\nu + \widetilde{\nu})\nabla\widetilde{\nu}\right] + c_{b2}\left(\nabla\widetilde{\nu}\right)^2\right\};$$

(4)

where $\nu_t = \widetilde{\nu}f_{v1}$ and

$$f_{v1} = \frac{\chi^3}{\chi^3 + c_{v1}^3}, \qquad \chi = \frac{\widetilde{\nu}}{\nu}, \qquad \widetilde{S} = |\Omega| + \frac{\widetilde{\nu}}{\kappa^2\widetilde{d}^2}f_{v2}, \qquad f_{v2} = 1 - \frac{\chi}{1 + \chi f_{v1}}.$$

(5)

Here $|\Omega|$ is the magnitude of the vorticity, and the function f_w is given by

$$f_w = g\left[\frac{1 + c_{w3}^6}{g^6 + c_{w3}^6}\right]^{1/6}, \qquad g = r + c_{w2}(r^6 - r), \qquad r = \frac{\widetilde{\nu}}{\widetilde{S}k^2\widetilde{d}^2}.$$

(6)

The constants in the model are $c_{b1} = 0.1355$, $\sigma = 2/3$, $c_{b2} = 0.622$, $\kappa = 0.41$, $c_{w1} = c_{b1}/\kappa^2 + (1 + c_{b2})/\sigma$, $c_{w2} = 0.3$, $c_{w3} = 2.0$ and $c_{v1} = 7.1$. For the RANS application, the length scale d is the distance from the wall, y_W.

The governing equations were solved on a Cartesian staggered grid. Conservative second-order finite differences were used for spatial discretization. A fractional-step method [10] with a second-order implicit Crank-Nicolson time-advancement for the wall-normal diffusion term and a third-order explicit Runge-Kutta method for the remaining terms was used for time integration. Periodic boundary conditions were used in the spanwise direction, convective conditions [21] at the outflow, and the freestream condition [15],

$$\frac{\partial\overline{u}}{\partial y} = 0; \quad \overline{v} = U_\infty\frac{d\delta^*}{dx}; \quad \frac{\partial\overline{w}}{\partial y} = 0;$$

(7)

at the upper boundary; here δ^* is the boundary layer displacement thickness and U_∞ is the freestream velocity. We calculated $d\delta^*/dx$ using a linear regression on the $\delta^*(x)$ distribution. The Poisson equation is solved by a direct solver based on spanwise Fast-Fourier Transforms followed by cyclic reduction. The code is parallelized using Message Passing Interface routines.

2.2.3 Turbulence generation method

The method used to generate inflow turbulence is the controlled-forcing method, described in detail in [9, 6]; here we summarize its main features, concentrating on the parameters, and in the following sections we will make important modification and generalization to that model. The turbulence generation method consists of two parts: the creation of synthetic turbulence, and the controlled forcing. The synthetic turbulence generation method of [1] is used to an unsteady velocity field at the inflow plane of the LES region. An intermediate velocity, v_i is first constructed, using a sum of sines and cosines with random phases and amplitudes:

$$v_i(x_j, t) = \sqrt{\frac{2}{N}}\sum_{n=1}^{N}\left[p_i^n \cos(\widehat{d}_j^n\widehat{x}_j^n + \omega^n\widehat{t}) + q_i^n \sin(\widehat{d}_j^n\widehat{x}_j^n + \omega^n\widehat{t})\right],$$

(8)

where

$$\widehat{x}_j = 2\pi x_j/L_b, \qquad \widehat{t} = 2\pi t/\tau_b,$$

(9)

are spatial coordinates normalized by the length- and time-scale of the turbulence. In the above, $\tau_b = \mathcal{K}/\varepsilon$ and $L_b = \tau_b V_b$ are the turbulence time- and length-scale, and $V_b = \mathcal{K}^{1/2}$ is the velocity scale. The random frequencies $\omega^n = N(1,1)$ are taken from a normal distribution $N(\mu, \sigma^2)$ with mean $\mu = 1$ and variance $\sigma^2 = 1$. The amplitudes are given by

$$p_i^n = \epsilon_{ijk}\zeta_j^n d_k^n, \qquad q_i^n = \epsilon_{ijk}\xi_j^n d_k^n$$

(10)

where ζ_i^n, $\xi_i^n = N(0,1)$, and

$$\widehat{d}_j^n = d_j^n\frac{V}{c^n}.$$

(11)

6

are modified wavenumbers obtained by multiplying the wavenumbers, d_i^n, by the ratio of the velocity scale $V_b = L_b/\tau_b$ to c^n, given by

$$c^n = \sqrt{\frac{3}{2}\langle u_l' u_m'\rangle \frac{d_l^n d_m^n}{d_k^n d_k^n}}. \tag{12}$$

The wave-numbers $d_i^n = N(0, 1/2)$ are chosen from a normal distribution with variance $1/2$, resulting in a three-dimensional spectrum that behaves like $d^4 \exp(-d^2)$. Although the wave-numbers d_i^n are distributed isotropically in a sphere, dividing them by c^n tends to elongate those wave-numbers that are most closely aligned with the largest component of the Reynolds-stress tensor, and contract those aligned with the smaller ones. This results in a more physically realistic spectrum of turbulence, with eddies that (near the walls) are more elongated in x, and tend to be more spherical in the channel center. The synthetic turbulent fluctuation field is finally reconstructed by a tensor scaling:

$$u_i' = a_{ik} v_k \tag{13}$$

where a_{ik} is the Cholesky decomposition of the Reynolds-stress tensor. The method requires turbulence time- and length-scale, $\tau_b = \mathcal{K}/\varepsilon$ and $L_b = \tau_b \mathcal{K}^{1/2}$ (where $\mathcal{K}$ is the turbulent kinetic energy and ε the dissipation) that must be supplied by the RANS solution. When the SA model is used, following [2, 18], we estimate k and ϵ from

$$\sqrt{C_\mu}\mathcal{K} = |\langle -u'v'\rangle|; \qquad \epsilon = C_\mu \mathcal{K}^2/\nu_T. \tag{14}$$

The controlled-forcing method consists of a forcing term added to the wall-normal momentum equation that amplifies the velocity fluctuations in that direction, thus enhancing the production term in the shear-stress budget. The forcing amplitude is determined by a PI controller, which has two components: a proportional part and an integral one. The two outputs are added together to form the actuating signal of the system to control, the Navier-Stokes equation system.

The error is defined as

$$e = \langle u'v'\rangle^{target} - \langle u'v'\rangle^t \tag{15}$$

where $\langle u'v'\rangle^{target}(x_o, y)$ is the desired Reynolds shear stress at the control plane $x = x_o$ obtained from the RANS solution and which is the target of the control procedure; $\langle u'v'\rangle^t(x_o, y, t)$ is the Reynolds shear stress, averaged over some time interval. All terms are evaluated at the control plane x_o, and may be function of y, z and t. The magnitude of the forcing is then set to

$$f^{CF}(x_o, y, z, t) = r(y, z, t)\left[u(x_o, y, z, t) - \langle u\rangle^t(x_o, y, z, t)\right] \tag{16}$$

where

$$r(t) = K_P e(t) + K_I \int e(t')dt' \tag{17}$$

is the output of the PI controller. The significance of the two constants, K_P and K_I and the optimal value of the length of the time average window, will be discussed later. The forcing so defined is added to the y-momentum equation. Enhancing the v' fluctuations through events with large u' [the term in square brackets in (16)] has the effect of accelerating the production of Reynolds shear stress.

3 Analysis of the controller parameters

3.1 Preliminary study in a flat-plate boundary layer

Although the controlled-forcing method has shown some promise, its development so far has been heuristic. The first step of our research consisted in investigating more closely the link between the model parameters and the flow physics, to establish the robustness and stability of the method and to improve its performance. The test case used to evaluate the parameters in the model was a flat-plate boundary layer; then, the results were extended and generalized to more complex flows with different characteristic time- and length-scales, such as a flat-plate boundary layer subjected to favorable and adverse pressure gradients, and a three-dimensional boundary layer.

The controller described above has three parameters: the constants K_P and K_I and the width T_{ave} of the averaging window used to obtain $\langle u'v' \rangle^t$. In past applications [39, 9, 6] no investigation was carried out in which they were systematically varied. In this section we examine the transient and steady-state responses of the flow to these parameters, and relate them to physical properties of the flow, as well as to each other. The target is to choose them to obtain statistically steady-state Reynolds stresses that match the desired ones in a short distance without destabilizing the Navier-Stokes equation system. While we cannot claim that to have found true optimal values of these parameters, we will refer to our choice as "optimal" if it gives realistic turbulence in the shortest distance, and with the shortest transient.

We test them in a flat-plate, zero-pressure-gradient (ZPG) boundary layer. First, we carried out the reference LES on a domain $240\delta_o^* \times 25\delta_o^* \times 25\delta_o^*$ in the streamwise, wall-normal and spanwise directions, respectively; here δ_o^* is the displacement thickness at the inflow. From this calculation, the time-averaged Reynolds shear stress and the turbulence scales were extracted at $x/\delta_o^* = 80$. At this section a LES of dimension $120\delta_o^* \times 25\delta_o^* \times 25\delta_o^*$ with the synthetic turbulence generation and the controlled forcing at the inflow began. In this way it was possible to analyze the effect of K_I, K_P and T_{ave} without the errors introduced by a RANS model. The control planes were distributed over a length of $27.5\delta_o^*$ downstream of the interface in the LES domain, with a spacing between planes of one boundary-layer thickness to allow the flow to re-adjust after the forcing (test calculations in which the forcing was distributed continuously had also carried out, with no significant differences [7]). The inflow Reynolds number (based on freestream velocity U_o and displacement thickness) was $Re_\delta^* = 1000$. The grid spacings in the streamwise and spanwise directions were $\Delta x/\delta_o^* = 1.25$ and $\Delta z/\delta_o^* = 0.385$, while 64 points were used in the wall-normal direction (with $y_{min}^+ \approx 1.0$). The recycling and rescaling method of Lund [15] was used as inflow boundary condition for the reference LES. This resolution is sufficient to ensure accurate prediction of the mean velocity and Reynolds stresses [8].

PI controllers give a robust performance over a wide range of operating conditions and are widely used due to their easy implementation. They are frequently used when the mathematical model of the system to control is complex or unavailable, in which case the parameter tuning can be based on semi-empirical rules. In unknown non-linear system, however, the primary target of the parameter tuning is the stabilization of the controlled system, and, marginally, the steady state performance. In the controlled-forcing turbulence generation method, the system to control is the filtered NS equation system with a dynamic subgrid model. The target is the Reynolds shear stress obtained from the RANS solution. The output of the system is the instantaneous $u'v'$ correlation, averaged using an appropriate filter.

We begin by discussing the moving-average (MA) filter. In the classical terminology used in the feedback control theory, this block is called "Measuring device": the instantaneous velocity fluctuations u'_i are the inputs to the MA block, which outputs an appropriate time-averaged Reynolds stress that can be compared to the target obtained from the RANS. We use an exponentially weighted moving-average filter, which places more emphasis on the most recent data available. At time-step k we use the following expression:

$$\langle x_k \rangle^t = \left(1 - \frac{\Delta t}{T_{ave}} \right) \langle x_{k-1} \rangle^t + \frac{\Delta t}{T_{ave}} x_k \tag{18}$$

Δt is the time-step, and x is the data to average.

The value of $\Delta t/T_{ave}$ determines the memory of the filter. We define an attenuation time T_d as the time after which the contribution of the signal at some time to the averaged data is negligible (say, 5% of the original contribution). It is easy to show that, in this case,

$$\frac{T_d}{T_{ave}} = \frac{\Delta t}{T_{ave}} \frac{\log 0.05}{\log \left(1 - \frac{\Delta t}{T_{ave}} \right)}; \tag{19}$$

since $\Delta t >> T_{ave}$, (19) gives $T_{ave} \simeq T_d/3$. We expect that T_d should be of the order of a large-eddy turnover time (LETOT), which results in $T_{ave} \simeq 10\delta^*/u_\tau$ in the present calculation. Values much larger than this result in long transients, as the error affects the input to the forcing for a long time, and the forcing does not adjust rapidly enough to the present flow conditions, but is strongly affected by past events. This is shown in Figure 4(a) where the domain-averaged TKE is plotted as a function of time; in all the calculations we used values of K_P and K_I found to give stability to the whole system (see the next subsection), except for one case in which we employed the values used in [9, 6].
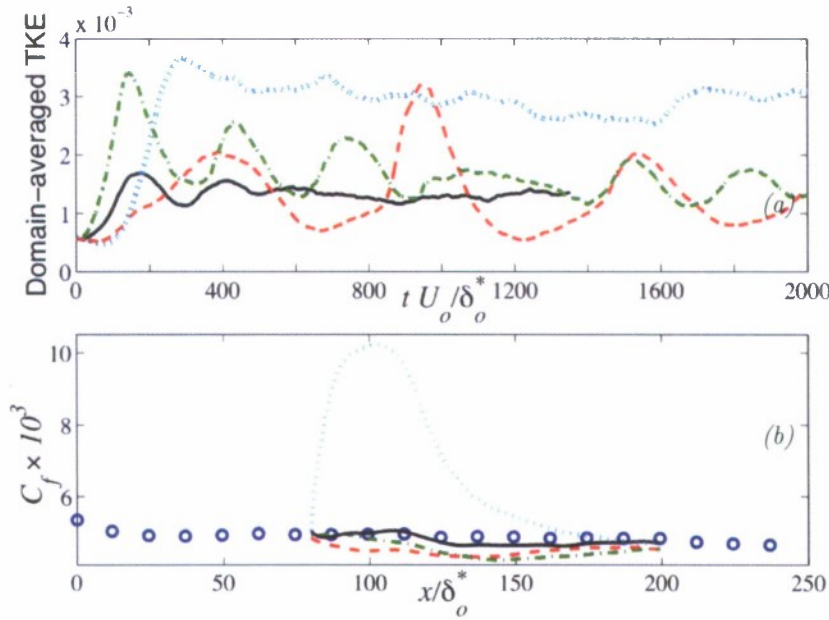
8

Figure 4: *(a)* Domain-averaged turbulent kinetic energy for $\cdots\cdots$ $T_{ave} = 1, K_I = 5, K_P = 30$; —— $T_{ave} = 10, K_I = 5, K_P = 30$; $---$ $T_{ave} = 100, K_I = 1, K_P = 1$; $-\cdot-$ $T_{ave} = 100, K_I = 5, K_P = 30$. *(b)* C_f for the reference LES ($\circ$) and the cases shown in *(a)*.

A longer transient can be observed with $T_{ave} = 100$ compared with $T_{ave} = 10$. With the lower values of K_P and K_I used in early applications of this method the transient is quite long, the magnitude of the oscillations is significant, and flow statistics require very long averaging times. Note that the value of K_I and K_P used in [9, 6] are at the limit of the stability. A stable choice of K_P and K_I, on the other hand, reduces the amplitude of the fluctuations even if a high value of T_{ave} is used. A low value of T_{ave} results in incorrect prediction of the flow: the short averaging gives values of $\langle u'v'\rangle^t$ that are too far from a stationary sample, and may result in excessive forcing being applied even if the flow has reached a realistic state.

In Figure 4*(b)* the skin-friction coefficient $C_f = 2\tau_w/\rho U_\infty^2$ (where τ_w is the wall stress) is shown for the same cases. Excessively small values of T_{ave} result in incorrect steady state results, while the other values of T_{ave} are in reasonable agreement with each other. The case with $T_{ave} = 10$ (*i.e.*, T_d of the order of one LETOT) gives somewhat more accurate statistics and a much shorter transient (and reduced CPU costs). Unless explicitly specified, $T_{ave} = 10$ for all following cases.

On a related note, it should be mentioned that previous applications of the controlled forcing method [39, 9, 6] used spanwise averaging (in addition to the time-averaging) to supply a smoother signal to the forcing. The results shown above, however, indicate that this requirement must be balanced by the need to have an error that reflect more closely the local and instantaneous conditions of the flow. We performed calculations in which no spanwise averaging was performed and compared them to a simulation in which the $u'v'$ correlation is averaged in the spanwise direction as well as in time (Figure 3.1). We observe more rapid adjustment of the flow towards the reference LES, as the forcing is more responsive to the local state of the flow.

We now turn our attention to the other parameters of the PI controller to evaluate their influence on the transient time, steady-state results and stability of the system. In general a proportional controller affects the rise-time and the transient time of the dynamic system: it modifies the bandwidth of the frequency response of the closed loop system and the gain of the zero frequency. If K_P is large, the output of the integral block is more sensitive to the high-frequency variation of the error, and the stability of the system can be affected. The integral control, on the other hand, gives a large gain at low frequency and reduces the break frequency (the point where the amplitude spectrum of the transfer function is zero); its effect is to eliminate the steady-state error and attenuate the high-frequency disturbances. In fact, the output of the
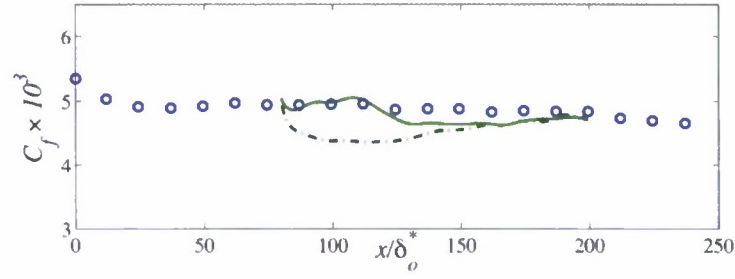
Figure 5: Skin friction coefficient C_f with $K_I = 5$ and $K_P = 30$; $-\cdot-$ $\langle u'v' \rangle^t$ is spanwise-averaged; $\underline{}$ $\langle u'v' \rangle^t$ is not spanwise-averaged.
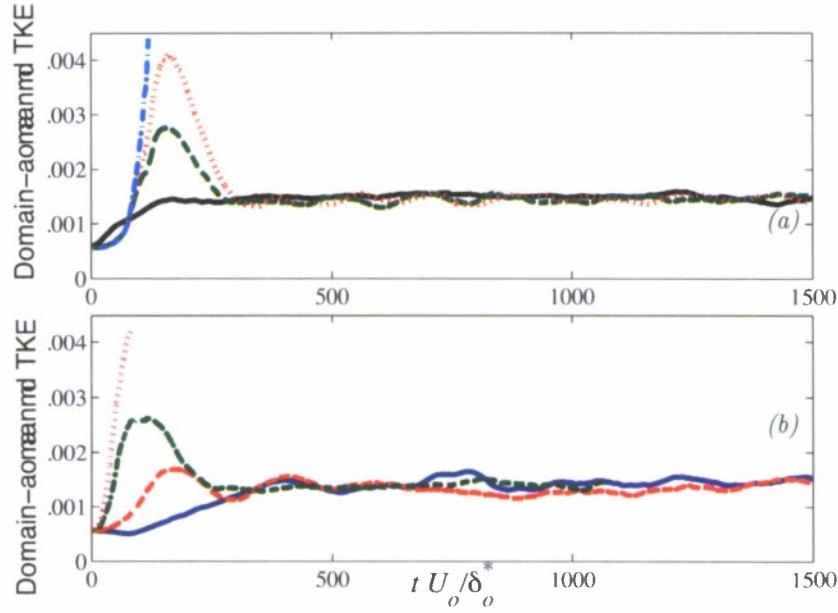
Figure 6: Domain-averaged turbulent kinetic energy. (a) $K_I = 5$ and $-\cdot-$ $K_P = 0$; $\cdots\cdots$ 15; $---$ 30;$\underline{}$ 500; (b) $K_p = 30$ and $\underline{}$ $K_i = 1$, $---$ 5, $-\cdot-$ 20, $\cdots\cdots$ 30.

integral control will change over time as long as an error exists, but the phase lag between the input and output of the integral block increases for all of the frequencies (the phase of the integrator block starts at -90°). If K_I is large, the phase lag is extended to higher frequency, so the system can became oscillatory and potentially unstable.

Figure 6 shows how the transient is affected by K_P and K_I. If $K_P = 0$ (only the integral control is activated) the calculation diverges: in the initial transient the forcing is proportional to $e(t')dt'$ and the initial time-step is small because of the initial unphysical flow in the computational domain. Because of the small time-step the integral action is weakened, so the integral control needs a longer time before it can give a correct control signal. As the simulation advances, however, the time-step is further decreased because no fast correction is present in the domain, so the correct integral action is even more delayed until the simulation goes unstable. The case of high K_P is the opposite: as soon as the simulation starts there is the fast correction due to the proportional control. Apart from the length of the transient, however, the steady-state results did not differ much in all the converged calculations, showing little sensitivity of the flow to the proportional controller (at least for $K_P > 1$).

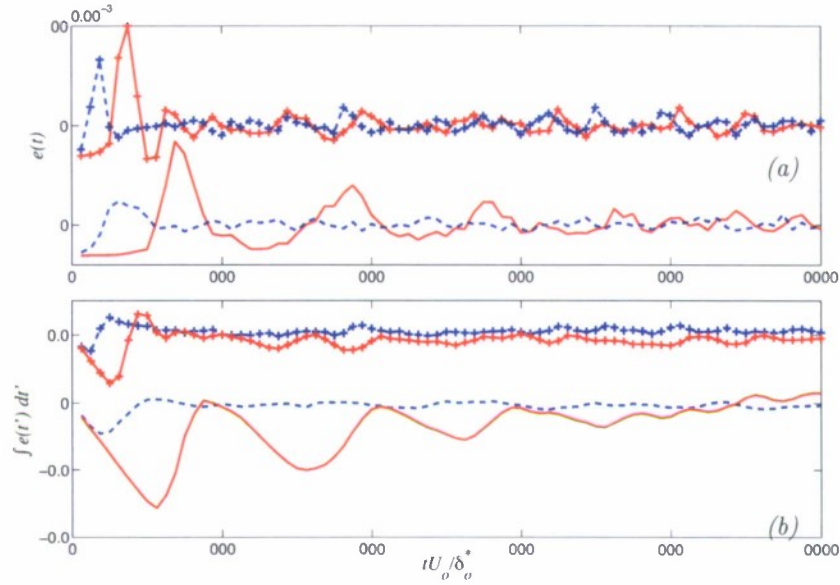Similarly, we found instability for $K_I \geq 30$, as can be expected by the theory of the PI feedback control.

10

Figure 7: *(a)* Instantaneous and *(b)* integrated error for $K_P = 30$ and $K_I = 5$ (lines) and $K_I = 20$ (lines with symbols). $---$ $y^+ = 13$; ——— $y/\delta_o^* = 4.5$. The curves for $K_I = 20$ are shifted upwards by 0.005 in *(a)* and 0.1 in *(b)*.

If K_I was close to zero, only the proportional control was activated and the steady state error (the difference between the desired Reynolds stress and the one obtained from the calculation) was large. Figure 7 shows the error and its integral at two locations, one in the wall layer, the other in the outer region of the boundary layer, for $K_P = 30$ and two values of K_I. Increasing K_I reduces the amplitude of the dominant frequency of the error, as well as its amplitude, at least in the outer layer. Note, however, that the forcing signal (which has the integral error multiplied by K_I) does not change its magnitude.

As a result of the tests described in this section, we conclude that some localization of the error, both in time and space, is desirable. In fact, inclusion of non-local (in space or time) effects may potentially give instability to the entire system. In that sense, the use of distributed forcing as in [7] may result in longer development lengths because it uses non local information. Compared with previous work, we obtained improved results using a time-averaging window with a time-scale matching the LETOT of the flow, and removing the spanwise averaging. We observed that the controller coefficients mostly affect the length of the transient and the stability of the system; for a wide range of both K_I and K_P, however, the flow statistics are fairly insensitive to the parameter values. In the next section we will apply the method with the time-averaged window using the LETOT as a time-scale to different flows, to determine its performance (with the new coefficients) in actual cases.

3.2 Applications

3.2.1 Adverse-pressure-gradient boundary layer

Hybrid simulations were next carried out in an adverse-pressure-gradient (APG) boundary-layer that undergoes separation. The configuration of these simulations is similar to that of [6], with an inflow Reynolds number, $Re_{\delta^*} = 1260$, and a profile of V_∞ imposed at the top boundary that results in a significant deceleration of the flow (see Figure 8). Due to the strong adverse pressure-gradient, the flow separates; a favorable pressure gradient then closes the recirculation bubble. The Reynolds number of this calculation is lower than that of the DNS by Na and Moin [19], but calculations carried out at the same Reynolds number showed excellent agreement with the DNS data.

The computational domain used in the full-domain LES was $380\delta_o^* \times 64\delta_o^* \times 20\delta_o^*$ (a subscript o refers to values evaluated at the inflow location). This LES, which used the rescaling/recycling method at the inflow,
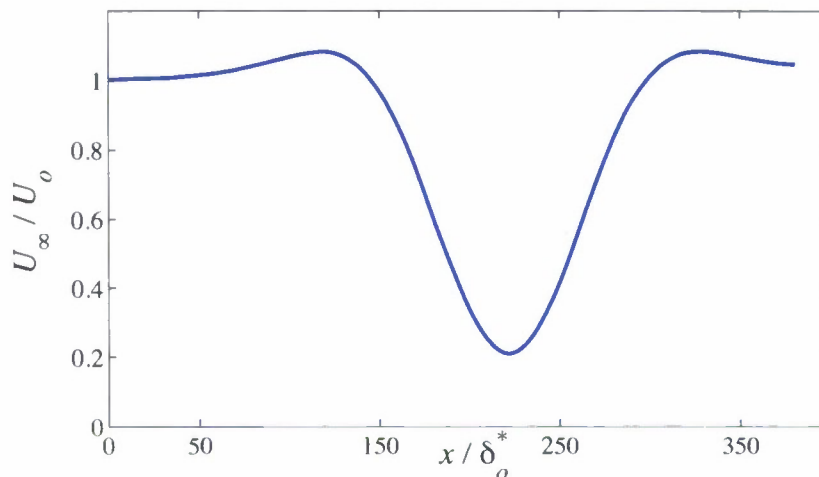
Figure 8: Freestream velocity for the adverse-pressure-gradient calculation.

had a grid of $384 \times 192 \times 64$. The RANS calculations for the hybrid cases were extended to cover the entire flow domain to remove difficulties of placing outflow boundary conditions close to reversed-flow regions; both SA and $\mathcal{K} - \epsilon$ models were used for the RANS solution. The LES region started at $x/\delta_o^* \approx 80$, and used the RANS data at that location for the synthetic turbulence generation, as well as target for the controlled forcing algorithm. The δ^*/u_τ obtained from the $\mathcal{K} - \epsilon$ model at the interface location was approximately 110, which agrees well with the value from the full LES. To match this value, T_{ave} was fixed to 38, so that the memory T_d was approximately 113. K_I was fixed at 5 and K_P to 30.

Figure 9 shows the C_f, mean velocity profiles and Reynolds shear stresses at three locations. As the boundary layer is subjected to the adverse pressure-gradient, C_f decreases until the flow separates at $x/\delta_o^* \approx$ 170. A weak separation bubble, which has a length of approximately $80\delta_o^*$, can be observed in the full-domain LES. The results from the RANS simulation in terms of C_f are close to those of the full LES. Switching to the LES is, however, beneficial (the prediction of C_f and the dimensions of the separation bubble are both more accurate). Shortly after separation (the second profile in Figure 9) some differences between the hybrid cases can be observed, whereas inside the separation bubble the LES gives similar results. In this flow, the amplification of turbulence in the separated shear layer acts as a powerful mechanism to accelerate the generation of realistic eddies.

Keating *et al.* [6] observed a much stronger dependence of the hybrid results on the accuracy of the RANS model (see Figure 11 in [6]). This effect is due to the use of suboptimal PI controller parameters and averaging window. With the more localized averaging used here, the initial decay of the wall stress that was observed by Keating *et al.* [6] does not occur.

Figure 10 shows contours of streamwise velocity fluctuations in a plane near the wall for the reference LES and a hybrid case. We observe a very rapid development of a physical streaky structure. The onset of separation (which is strongly affected by the flow state immediately before the separation occurs) is predicted well, and the length-scales of the flow in the separated-flow region are remarkably similar, confirming again the robustness and effectiveness of the method.

3.2.2 Favorable pressure-gradient boundary layer.

Simulations of a boundary layer subjected to a favorable pressure-gradient (FPG) were performed next. In this flow, if the acceleration is rapid enough, re-laminarization and re-transition of the flow may occur. The case studied here matches the experiments of [41]. The freestream acceleration (from $U_\infty = 1$ to $U_\infty \approx 3$) begins at approximately $100\delta_o^*$ and is completed by $450\delta_o^*$. The flow acceleration is achieved by imposing a streamwise velocity profile $U_\infty(x)$ at the top boundary of the domain [15]. Its magnitude was calculated from the acceleration parameter, $K = (\nu/U_\infty^2)(dU/dx)$, experimentally obtained from [41]. The acceleration parameter, K, and the free-stream velocity distribution $U_\infty(x)$ are the same as [6]. Since K exceeds the
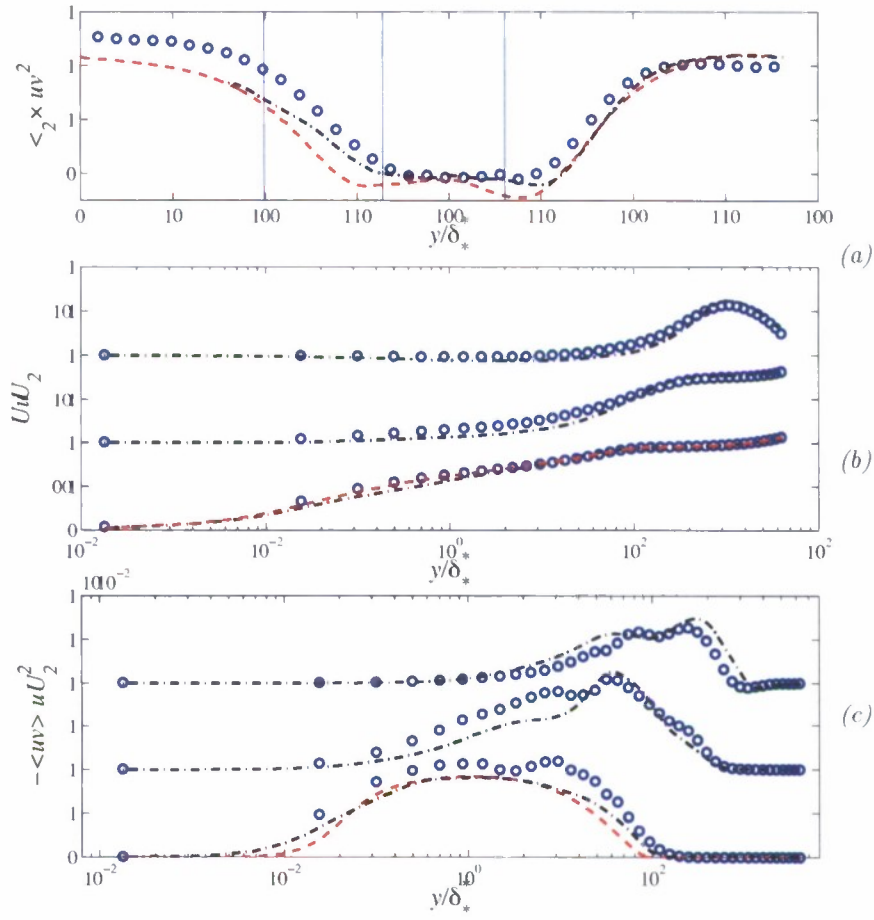
Figure 9: Adverse-pressure-gradient boundary layer. *(a)* Skin friction coefficient C_f *(b)* mean velocity profiles and *(c)* profiles of the Reynolds shear stress at the locations indicated by a vertical line in part *(a)*. ○ Reference LES; --- SA RANS; -·- Hybrid SA RANS/LES.
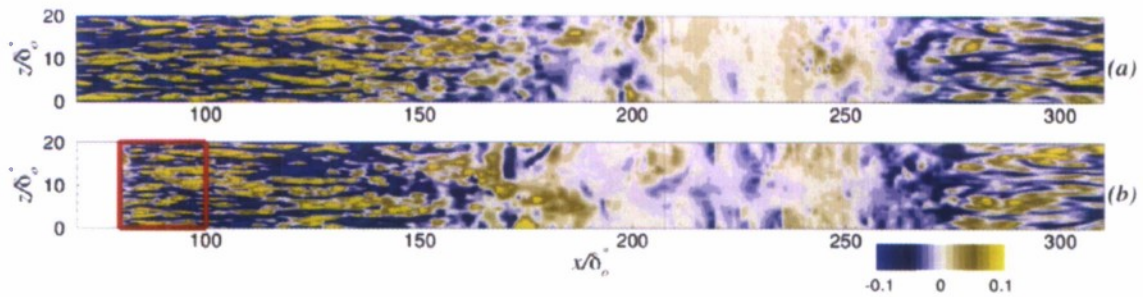

Figure 10: Streamwise velocity fluctuations in the APG boundary layer, in the $y/\delta_o^* = 0.09$ plane. *(a)* Reference LES; *(b)* hybrid $\mathcal{K} - \epsilon$/LES; the red rectangle indicates the region where the control is active.
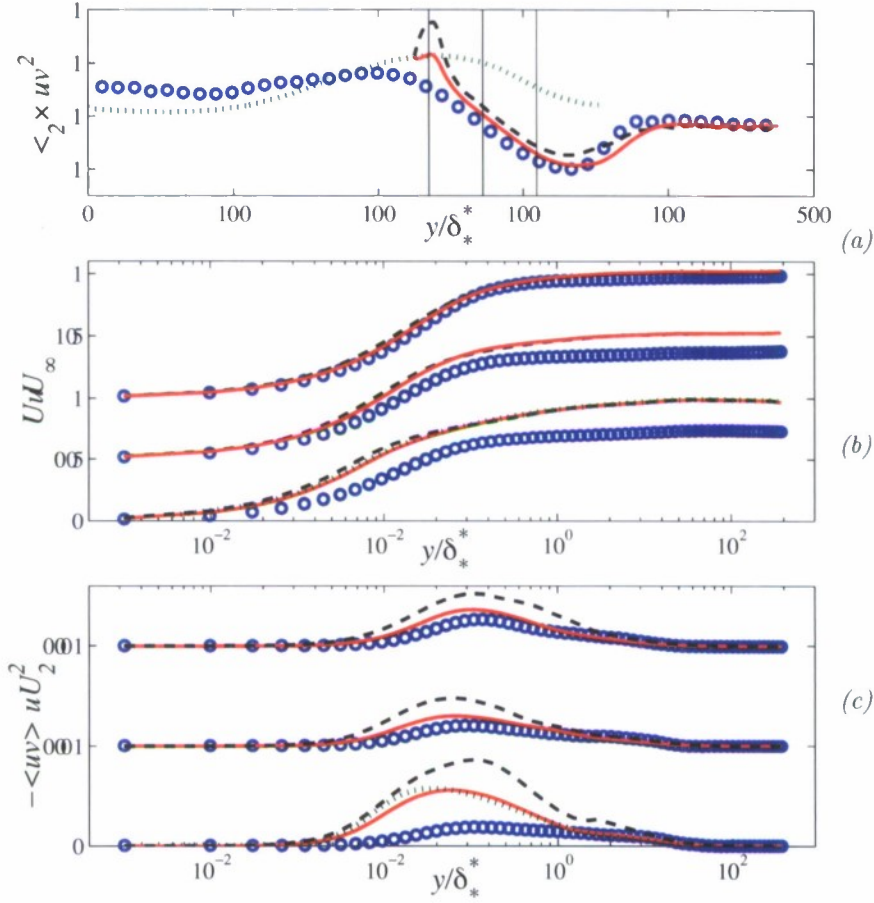
13

Figure 11: Favorable-pressure-gradient boundary layer. *(a)* Skin friction coefficient C_f *(b)* mean velocity profiles and *(c)* profiles of the Reynolds shear stress at the locations indicated by a vertical line in part *(a)*. ○ Reference LES; ⋯⋯ SA RANS; —— hybrid SA/LES, T_{ave} from LES data; - - - hybrid SA/LES, T_{ave} from RANS data; .

critical value for re-laminarization ($K_{crit} = 3.5 \times 10^{-6}$) for an extended region of the flow, turbulence is expected to be damped in the region of high acceleration. The flow then re-transitions once the acceleration is removed.

A full-domain LES was first performed using the rescaling/recycling method at an inflow Reynolds number, $Re_{\delta^*} = 1260$. For this simulation the domain length was $476\delta_o^*$, the width was $20\delta_o^*$ and the height was $20\delta_o^*$. A somewhat coarse grid ($512 \times 64 \times 64$) was used, since the comparisons were primarily being made between this full LES and a hybrid RANS/LES simulations. A previous LES study using a finer grid has shown excellent agreement with the experiments for this flow [4]; on the present grid, the qualitative behavior of the flow was captured accurately. although the re-transition following the release of the acceleration was slightly delayed. One hybrid calculations was performed that included a RANS domain $350\delta_o^*$ long, and an LES region that started at $x/\delta_o^* = 225$ and extended to $476\delta_o^*$ (*i.e.*, had a length $251\delta_o^*$). Synthetic turbulence with controlled forcing was introduced at the RANS/LES interface.

The SA RANS model gives significant modeling error, being unable to predict the relaminarization and the re-transition of the accelerating boundary layer correctly. Furthermore, the integral time-scale at the interface location was approximately $2 \, \delta_o^*/u_{\tau,o}$, while the value obtained from the full LES calculation is twice as large in the region where the control was applied. Two hybrid calculation were performed, one that used a value of T_d close to the time-scale predicted by the RANS (giving $T_{ave} = 1$), and another that
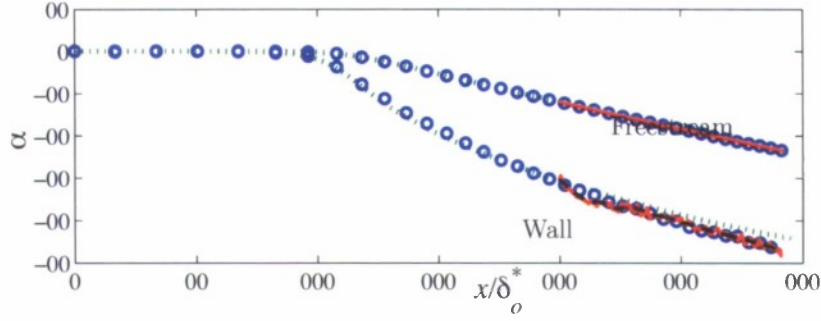
Figure 12: 3D boundary layer. Flow angle $\alpha = \tan^{-1} U/W$. ○ Reference LES. ⋯⋯ SA-RANS; − − − hybrid RANS/LES, error based on $\langle u'v' \rangle$; ——— hybrid RANS/LES, production-based error.

matched the LES time-scale ($T_{ave} \simeq 2.4$). Figure 11 compares the results of the various simulations. The mean data at the interface, which is supplied by the RANS, is not accurate; the controller tries to drive the LES towards the RANS region, but when T_{ave} is small a smooth $\langle u'v' \rangle$ cannot be obtained, and excessive forcing is applied, resulting in an initial overshoot of the skin-friction coefficient. Once the control is released, the flow adjusts fairly rapidly towards the full-domain LES. When a longer average is used, the controller is more successful in driving the LES shear stress towards the desired distribution (Figure 11(c)) and the LES adjusts more rapidly and with no overshoot. Note that this is a very challenging test case: RANS models cannot be expected to predict relaminarization accurately; furthermore, since the energy of the fluctuations is decreasing because of the acceleration, adding energy through the forcing term is moving the flow away from its equilibrium. Despite the fact that this can be considered an off-design application for the controlled forcing, the results are altogether acceptable.

3.2.3 3-D Boundary layer

Simulations were then performed on a 3D boundary layer obtained by applying a spanwise pressure gradient to a flat-plate boundary layer. The pressure gradient increased from zero, at $x/\delta_o^* = 100$, up to 1.5×10^{-3} at $x/\delta_o^* = 150$, and remained constant thereafter. The magnitude of the pressure gradient was set in such a way as to turn the flow by 45° near the wall and 24° at the free stream by the end of the domain. Figure 12 shows the turning angle near the wall and in the freestream.

Once again, two simulations were carried out: a full-domain LES, and one hybrid RANS/LES calculations. The computational domain of the reference LES was $291\delta_o^* \times 20\delta_o^* \times 20\delta_o^*$ with a grid of $720 \times 100 \times 292$. An inflow plane from a precursor simulation was used with an inflow Reynolds number of $Re_{\delta^*} = 1260$. Because of the turning of the flow, the grid had to be refined in the streamwise direction in the downstream area. We define a local coordinate frame with ξ in the flow direction and ζ in the lateral direction in the wall plane:

$$\Delta \xi^+ = \Delta x^+ \cos\alpha + \Delta z^+ \sin\alpha; \qquad \Delta \zeta^+ = \Delta x^+ \sin\alpha + \Delta z^+ \cos\alpha. \tag{20}$$

We maintained streamwise and spanwise grid resolutions of $\Delta \xi^+ < 50$ and $\Delta \zeta^+ < 13$. Here, α is the flow angle at the wall and wall units are defined using the resultant wall stress

$$\rho u_\tau = (\tau_{xy,w}^2 + \tau_{xz,w}^2)^{1/4}; \quad \tau_{xy,w} = \mu \left.\frac{\partial U}{\partial y}\right|_{y=0}; \quad \tau_{xz,w} = \mu \left.\frac{\partial W}{\partial y}\right|_{y=0}. \tag{21}$$

In the hybrid cases, the RANS equations were solved using the Spalart-Allmaras model. The LES region started at $x/\delta_o^* \approx 200$ where the flow angle was 32° near the wall and 12° in the free-stream. The SA model predicts a value of $\delta^*/u_\tau = 40$ at the RANS/LES interface; consequently, we set $T_{ave} = 14$ (corresponding to $T_d \simeq 42$).

One limitation of the current approach lies in the fact that the error is based on the Reynolds shear stress, which is not a coordinate-invariant quantity; in complex geometries or, as in this case, if $\langle u'v' \rangle$ is not the only non-zero off-diagonal component of the Reynolds stress tensor, the error definition might not be meaningful.
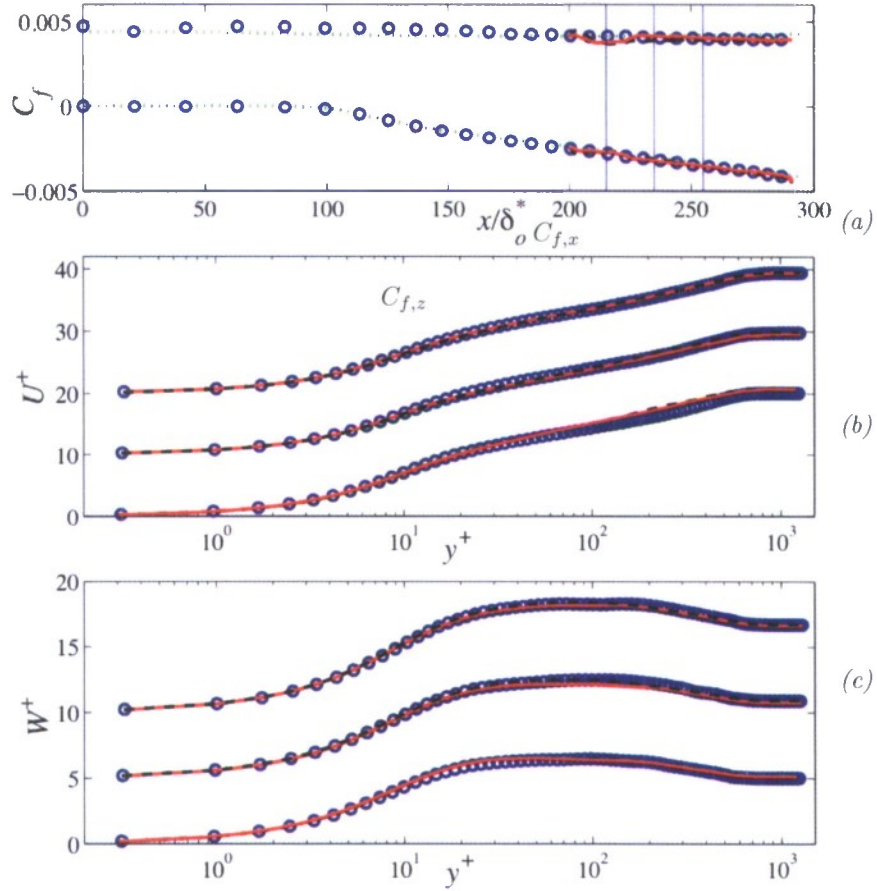
15

Figure 13: 3D boundary layer. *(a)* Streamwise and spanwise skin friction coefficients, $C_{f,x}$ and $C_{f,z}$; *(b)* mean streamwise velocity profiles and *(c)* mean spanwise velocity profiles at the locations indicated by a vertical line in part *(a)*. ○ Reference LES; ⋯⋯ SA RANS; − − − error based on $\langle u'v' \rangle$; —— production-based error.
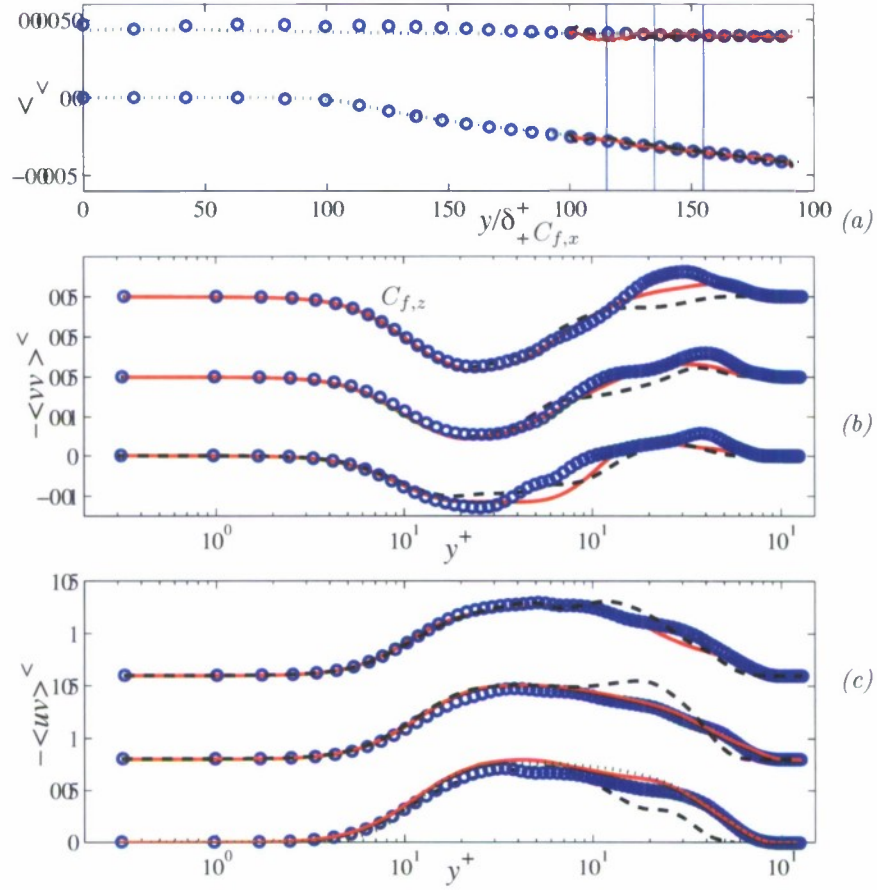
16

Figure 14: 3D boundary layer. *(a)* Streamwise and spanwise skin friction coefficients, $C_{f,x}$ and $C_{f,z}$; *(b)* mean $\langle v'w' \rangle$ Reynolds stress and *(c)* mean $\langle u'v' \rangle$ Reynolds stress at the locations indicated by a vertical line in part *(a)*. ○ Reference LES; ⋯⋯ SA RANS; − − − error based on $\langle u'v' \rangle$; —— production-based error.
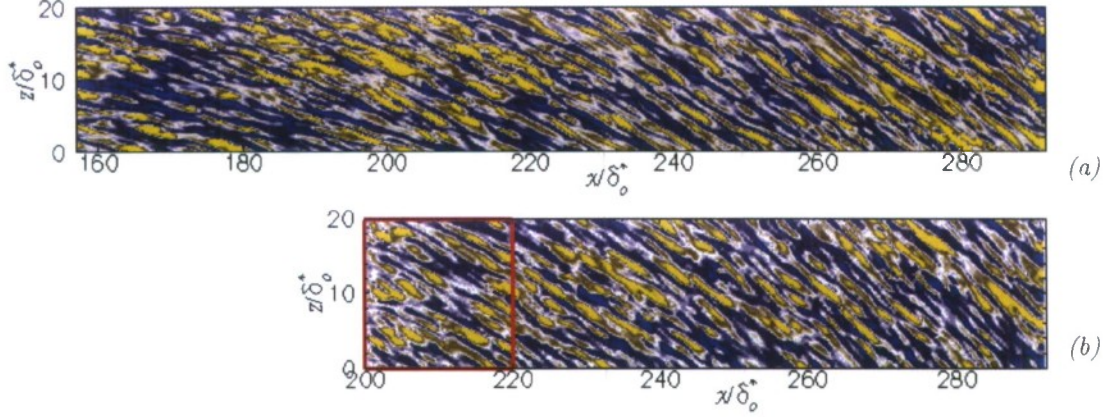
Figure 15: Contours of streamwise velocity fluctuations in a xz−plane near the wall, $y/\delta^*/o = 0.18$. *(a)* Reference LES (only part of the domain is shown); *(b)* hybrid RANS/LES.

The proposed RANS/LES merging approach is predicated on the RANS calculation being accurate in the interface region, which in practice restricts the interface to lie in a thin, attached shear layer, where the definition of directions along and normal to the shear layer is unique. Despite this practical observation, it would be desirable to develop a more universal error definition, and in particular one that is invariant to the choice of the frame of reference. One possible choice to satisfy this requirement is to base the error on the production of turbulent kinetic energy, which satisfies the desired invariance properties. Thus, we define a production-based error

$$e^P(y, z, t) = -\langle u_i' u_j' \rangle^{target} \langle S_{ij} \rangle^{target} + \langle u_i' u_j' \rangle^t \langle S_{ij} \rangle^t \tag{22}$$

(where the dependence on x_o, y, z and t has been omitted, and S_{ij} is the strain-rate tensor). We compared simulations with the production-based error defined above in addition to those with the standard definition of e.

Figure 13 shows the skin friction coefficient and mean velocity profiles in the streamwise and spanwise directions. The development of $C_{f,x}$ is similar to that of the ZPG case (with an initial decrease followed by a quick recover). For the lateral flow we observe remarkably good agreement with the reference simulation beginning from the end of the controlled region, approximately two boundary layer thicknesses downstream of the inflow. The principal shear stress, $\langle u'v' \rangle$ and the secondary ones $\langle v'w' \rangle$ develop quite rapidly (Figure 14). Notice that by adding the forcing into the v equation we amplify $\langle v'v' \rangle \partial W/\partial y$, i.e., the production of the secondary stress, as well as the production of $\langle u'v' \rangle$.

Figure 15 shows streamwise velocity fluctuations in a plane parallel to the wall. We observe again a very rapid build-up of the streaky structure starting from the synthetic turbulence.

3.3   Conclusions

We have further developed the controlled-forcing method for turbulence generation at RANS/LES interfaces. The method has shown itself to be robust and efficient. By studying the zero-pressure-gradient boundary layer (which, despite its simplicity is one of the most challenging cases examined) we developed guidelines for the determination of the parameters of this method.

We found that it is extremely important that the data compared with the target Reynolds stress (or production) is averaged over a time interval consistent with the physics of the flow. Averaging over a time interval of the order of the local integral time-scale resulted in shorter transient and more rapid development of physically realistic turbulent eddies. The inclusion of non-local information (as is the case when spanwise averaging is also applied) is generally not beneficial.

The controller constants K_P and K_I play a less significant role. Giving excessive weight to the integral error, or insufficient one to the proportional part, results in instabilities of the flow. For a wide range of values of K_P and K_I, on the other hand, the controller was stable and the flow statistics were insensitive to the constants.

Of the flows examined, we found the zero-pressure-gradient and favorable-pressure-gradient boundary layers to be the most challenging: in the zero-pressure-gradient case no external mechanism amplify the instability of the flow, so that the generation of turbulence is entirely due to the synthetic turbulence and controlled forcing; since the latter is less effective in the outer layer (where the turbulence production mechanisms are weaker), we observe the slow development of the outer layer. The favorable-pressure-gradient boundary layer presents a different set of problems: The acceleration results in relaminarization of the flow. Therefore, the injection of energy due to the forcing drives the flow in the wrong direction. In addition, RANS models are not very accurate in the strong acceleration region, which results in three sources of error: first, the mean velocity at the interface is far from the result obtained with the full-domain LES. Second, the target stresses are not close to the "correct" ones; thus, the controller drives the solution towards an incorrect one. Finally, the time-scale obtained from the RANS is substantially different from that obtained from the reference calculation, so that the moving average is suboptimal.

The method worked well in the adverse-pressure-gradient case, in which the deceleration (and, to an even greater extent, the separation) amplifies the disturbances, thus aiding the generation of turbulent eddies. This result is consistent with the findings of Terracol [40], who had some success using synthetic turbulence generation in the adverse-pressure-gradient region on the suction side of a turbine blade. In the 3D boundary layer the turning of the streamline imposed by the spanwise pressure gradient drives the lateral flow, with secondary stresses that develop from nearly zero at the RANS/LES interface. The controller proves to be able to seed the turbulence enough that the growth of the secondary stresses, and hence the lateral mean velocity profile, can be predicted accurately.

In summary, we have shown that the controlled forcing method is robust and efficient. The least favorable results are obtained in mildly unstable flows like the ZPG pressure gradient, or in re-laminarizing ones. Even in these situations, within 5 boundary layer thicknesses of the end of the control region a realistic flow was established. In realistic applications, especially in curved flows and in adverse pressure gradients (an important class of applications) the controlled forcing gives very rapid development of realistic eddies. The application to a realistic complex flow (the flow over a turbine blade or airfoil, for instance), is the next step in the development of this method. An important extension, that also needs to be investigated, is that to compressible flows. In particular, it needs to be shown that the energy added to the system through the forcing remains as kinetic energy and is not transferred to internal energy.

4 Application to separated flows

4.1 Introduction

The target application of this research is the application of hybrid methods to flows (such as those sketched in Figure 2) in which separation may be unsteady or mild; in these cases one would want to switch from the RANS to the LES method upstream of the separation, to capture the eddies generated in that region. In this type of flows, however, an accurate prediction of the turbulent momentum transport is extremely important, since errors in the mean velocity profile can cause premature separation [24, 23]). This phenomenon is one of the acknowledged weaknesses of the Detached Eddy Simulation approach(see the recent review by Spalart [37]). The rapid generation of turbulent eddies is, therefore, critical.

We will consider the flow configuration shown in Figure 16. The geometry consists of a flat plate followed by a smoothly contoured ramp and another flat plate region. Experiments on this geometry were conducted by Song and Eaton [33]. As the turbulent boundary layer goes over the ramp, the flow expands, creating an adverse pressure gradient that causes the flow to separate on the ramp. The flow subsequently re-attaches on the flat plate region. Experimental data are available at various streamwise locations: upstream of the ramp, at the point where the ramp begins, at the separation point, at the trailing edge of the ramp, at the re-attachment point and at two locations in the recovery region. Velocities are normalized by the free-stream velocity at the reference location $x_R = -2$. Although geometrically simple, the contoured ramp is a challenging test case. Downstream of the equilibrium boundary layer the adverse pressure gradient and
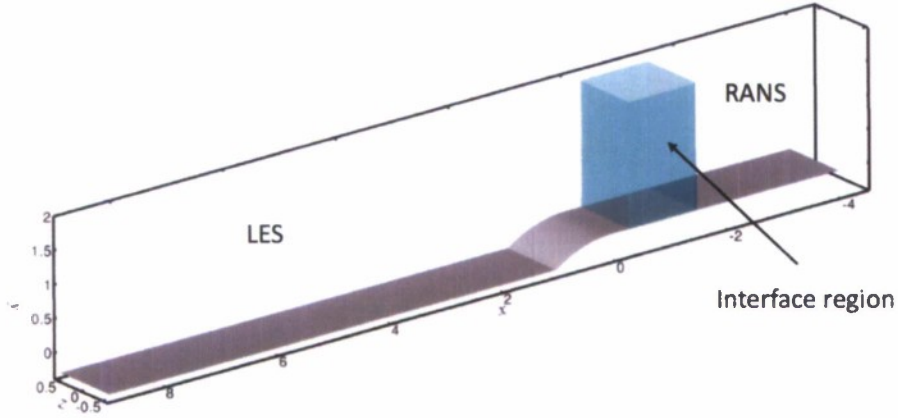
Figure 16: Sketch of the hybrid RANS/LES of the flow over a contoured ramp.

streamline curvature affect turbulence significantly. The separation is due to the pressure gradient, and was found to be highly unsteady and three-dimensional. Incorrect prediction of the separation point, moreover, affects the downstream development of the flow quite significantly through the instability of the separated shear layer. As mentioned above, premature separation is often the result of the application of hybrid RANS/LES methods to flows with shallow separation [37].

The hybrid calculation uses the Spalart-Allmaras [34] turbulence model in the RANS region. The same model is used in the LES region, but the length scale is modified (see below) to yield an SGS model of the type used in most DES applications. The interface between the RANS and LES regions, shown in light blue in Figure 16, is where the forcing is applied.

In the following we will first describe the geometry and the configuration parameters. Then, we will present the equations of motion, with the addition of the forcing terms; we will then present the turbulence models used for the calculation. Finally, we will present and discuss the results of the hybrid calculations.

4.2 Problem formulation

4.2.1 Governing equations

The governing equations are the filtered Navier-Stokes equations, with the addition of a forcing term, f_i, active only in the forcing region:

$$\frac{\partial \overline{u}_i}{\partial x_i} = 0 \tag{23}$$

$$\frac{\partial \overline{u}_i}{\partial t} + \frac{\partial \overline{u}_j \overline{u}_i}{\partial x_j} = \frac{1}{Re} \frac{\partial^2 \overline{u}_i}{\partial x_j \partial x_j} - \frac{1}{\rho} \frac{\partial \overline{p}}{\partial x_i} - \frac{\partial \tau_{ij}}{\partial x_j} + f_i \tag{24}$$

The forcing term is set to zero everywhere, except in a region immediately downstream of the RANS/LES interface. It is designed to generate velocity fluctuations analogous to those introduced through the synthetic turbulence generation described in Section 2.2.3, and to enforce the controlled-forcing technique described there. Therefore, we let the force be given by

$$f_i = -\frac{D(\overline{u}_i + u_i')}{Dt} + \delta_{i2} f_i^{\mathrm{CF}}, \qquad x_{1\mathrm{F}} < x < x_{1\mathrm{F}} + a\delta_{\mathrm{ref}}, \tag{25}$$

where u_i' are the synthetic turbulence fluctuations defined by (8-13), f_i^{CF} is the controlled forcing added to the y-momentum equation only and defined by (15-17), x_{IF} is the location of RANS/LES interface, a is a parameter which defines how far the synthetic turbulence forcing is applied from the RANS/LES interface, and δ_{ref} is the boundary layer thickness at the reference location.
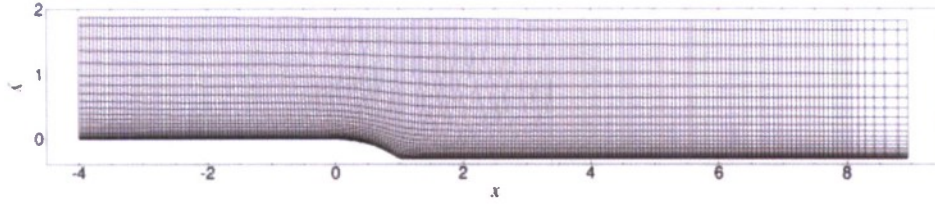
Figure 17: Computational grid used for the hybrid calculations. Only every 5th grid line is shown.

4.2.2 Turbulence model

In this calculation, the Spalart-Allmaras model, described in Section 2.2.2, is used both in the RANS and in the LES regions. In the RANS region, the length-scale $\tilde{d}$ is given by the distance from the wall, y_W; in the LES region it is equal to

$$e\tilde{d} = C_{\text{DES}}\Delta \tag{26}$$

where $C_{\text{DES}} = 0.65$ and $\Delta = \max(\Delta x, \Delta y, \Delta z)$. The resulting model relaxes to the Smagorinsky model [31, 14] when the small scales are in equilibrium, but is better able to include non-equilibrium effects through the use of the transport equation for the eddy viscosity. The transition between RANS and LES mode is achieved by decreasing the length scale from its RANS value to LES value linearly over a streamwise distance of δ_{ref} after the nominal interface, $x = -2$.

4.2.3 Geometry and problem parameters

The governing differential equations (23), (24) and (4) are discretized on a non-staggered grid using a curvilinear finite volume code. The method of Rhie and Chow [25] is used to avoid pressure oscillations. Both convective and diffusive fluxes are approximated by second-order central differences. A second-order semi-implicit fractional-step [10] procedure is used for the temporal discretization. The Crank-Nicolson scheme is used for the temporal discretization of wall-normal diffusive terms, and the Adams-Bashforth scheme is used for the temporal discretization of all the other terms. Fourier transforms are used to reduce the three-dimensional Poisson equation into a series of two-dimensional Helmholtz equations in wavenumber space, which are then solved iteratively using the Biconjugate Gradient Stabilized (BCGSTAB) method. The code is parallelized using the MPI message-passing library and the domain-decomposition technique, and has been extensively tested by Silva Lopes and Palma [29] in isotropic turbulence and by Silva Lopes *et al.* [30] in an S-shaped duct.

The geometry used for the present calculation is shown in Figures 16 and 17. In the numerical calculations, all the lengths are normalized by the ramp length, $L_R = 70$ mm. The flat plate section preceding the ramp is $2L_R$ long; the radius of curvature of the ramp is $1.814L_R$, its height is $0.3L_R$. In the numerical calculations, the flat plate region following the ramp has a length of $6L_R$ followed by a buffer zone for the outflow boundary. The computational domain height is $1.8714L_R$ which is same as the wind tunnel height. To save computational cost, the upper boundary layer near the top wall is not resolved but a free slip boundary condition is used.

The grid used for the present calculations, shown in Figure 17, uses $834 \times 90 \times 180$ grid points. In terms of the friction velocity at the reference location $x = -2$, the grid spacing along streamwise and spanwise directions are $\Delta x^+ = 20$ and $\Delta z^+ = 8.33$ which is sufficient for a wall-resolved LES calculation. The mesh is refined in the separation region and near the wall. The Reynolds number of the calculation was 1140 (based on U_R, the freestream velocity at the reference location $x = -2$ and the momentum thickness θ).

4.3 Results and discussion

We performed four calculations: first a full LES of the entire domain. In this case we used planes of data from a separate calculation as inflow condition. Then, we performed three hybrid cases. In the first, no forcing was applied: $f_i = 0$ in (24). The perturbations present in the flow from the initial condition (which was one
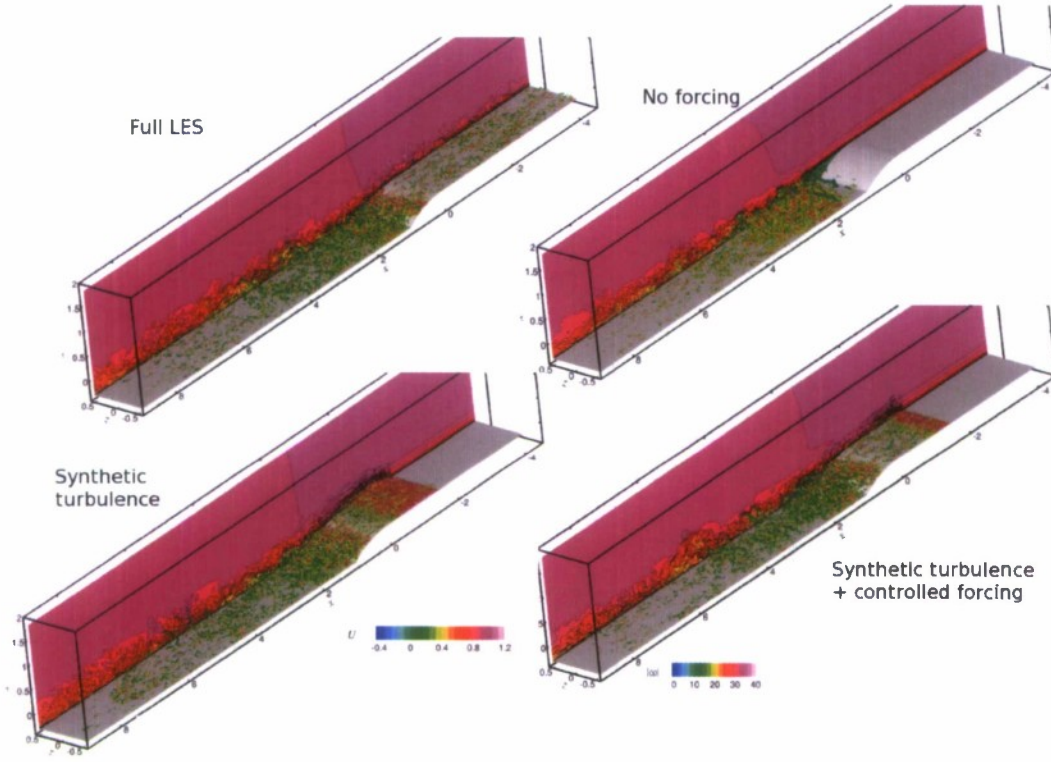
21

Figure 18: Flow visualization for the reference LES and hybrid calculations. The side plane shows contours of the time-averaged streamwise velocity U, while the isosurfaces of $Q = 60U_R^2/L_R^2$ (coloured by the vorticity magnitude $|\omega|$) highlight the vortical structures.

of the fields of the full LES) were allowed to be amplified and transition in the LES region. Another hybrid case used the synthetic turbulence but no controlled forcing: $f^{\mathrm{CF}} = 0$ in (25). In this case only random fluctuations were introduced by the forcing. The force f_i was active for a length $L_f = 5\delta_{\mathrm{ref}}$ downstream of the interface (shorter distances were tried, but were found to be insufficient to generate sustained turbulent eddies). Finally, we performed a calculation in which f_i included both synthetic turbulence and controlled forcing. The forcing in this case was active only for a length $L_f = 3\delta_{\mathrm{ref}}$.

Figure 18 shows visualizations of the flow for the four cases. The turbulent eddies are visualized by isosurfaces of the second invariant of the velocity gradient,

$$Q = -\frac{1}{2}\left(\frac{\partial \overline{u}_i}{\partial x_j}\frac{\partial \overline{u}_j}{\partial x_i}\right) = -\frac{1}{2}\left(\overline{S}_{ij}\overline{S}_{ij} - \overline{\Omega}_{ij}\overline{\Omega}_{ji}\right). \tag{27}$$

(where Ω_{ij} is the large-scale rotation-rate tensor), coloured by the vorticity magnitude.

In the reference LES one can observe that the flow upstream of the ramp contains coherent structures, highlighted by the contours of streamwise velocity and the vortical structures. Turbulence is enhanced first by the adverse pressure gradient, and further by the separation, leading to more (and stronger) coherent eddies in the initial part of the recovery region. In the hybrid calculation with no forcing the flow is smooth in the RANS region (as expected) but no eddies are generated in the LES region until separation occurs. The absolute instability of the separated shear layer naturally amplifies any perturbation present in the flow, so that sustained turbulence can be observed in the recovery region. The absence of eddies in the interface region, however, leads to quantitative inaccuracies, as will be shown below. One effect of the forcing is to create an unphysical flow in the interface region, with excessive generation of coherent eddies with very high vorticity (significantly higher than in the rest of the flow). As mentioned above, the forcing based
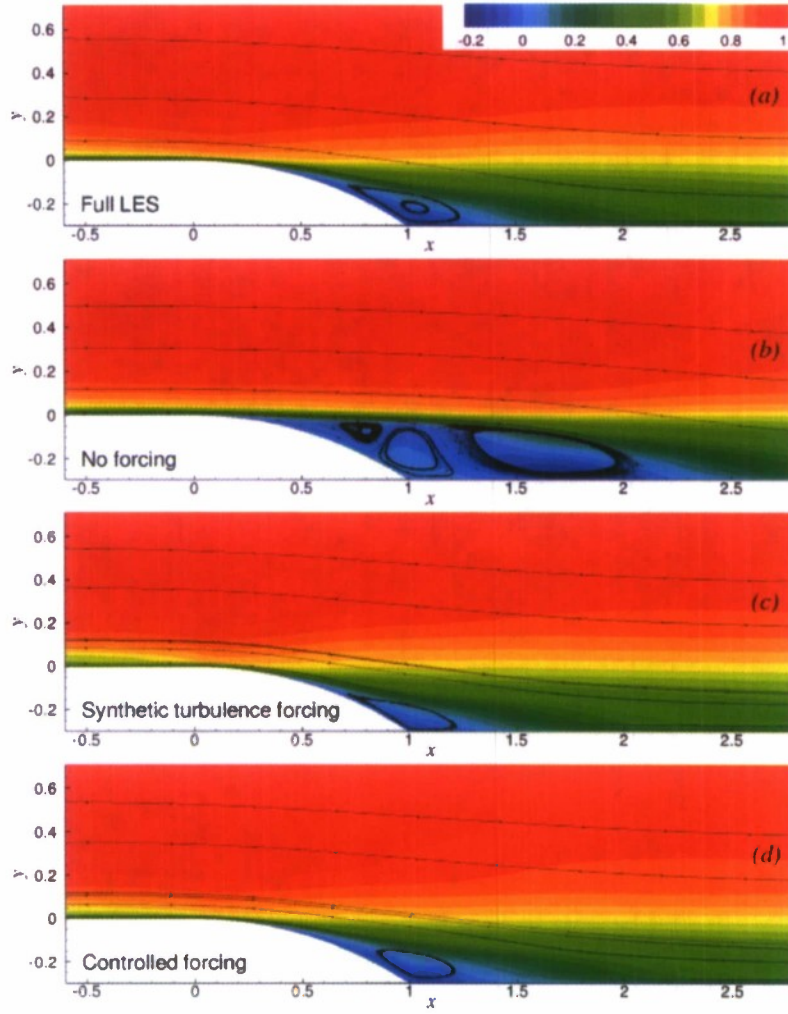
Figure 19: Contours of streamwise velocity and streamlines. *(a)* Full LES; *(b)* Hybrid RANS/LES, no forcing at the interface; *(c)* Hybrid RANS/LES, synthetic turbulence forcing at the interface; *(d)* Hybrid RANS/LES, synthetic turbulence and controlled forcing at the interface.

on synthetic turbulence needed to be applied in a longer region to generate sustained turbulence. When controlled forcing is applied, the extent of the unphysical region is much reduced. For both cases, however, the flow structure resembles that of the reference LES by the beginning of the ramp, and the separation and recovery regions appear realistic.

The effect of the lack of coherent eddies that cause the momentum transport is evidenced by the mean streamlines of the flow, Figure 19. Compared with the full LES, the case in which no forcing is applied at the interface has early separation (at $x_s \simeq 0.22$, rather than $x_s = 0.36$, as predicted by the full simulation). The recirculation region is also much longer, with a complex structure including one principal and two secondary bubbles. When forcing is applied at the RANS/LES interface the shape of the separated-flow region predicted by the hybrid calculations is in much better agreement with the full simulation. When the forcing based on synthetic turbulence only is used the separation is slightly delayed ($x_s = 0.41$ *vs.* 0.36), whereas when controlled forcing is also used the separation point is predicted correctly. The reattachment point is predicted slightly early ($x_r = 1.35$) when synthetic turbulence forcing only is used, whereas a value in agreement with the full LES ($x_r = 1.44$) is predicted when controlled forcing is used.

The qualitative discussion based on the flow visualization is supported by the quantitative comparisons.
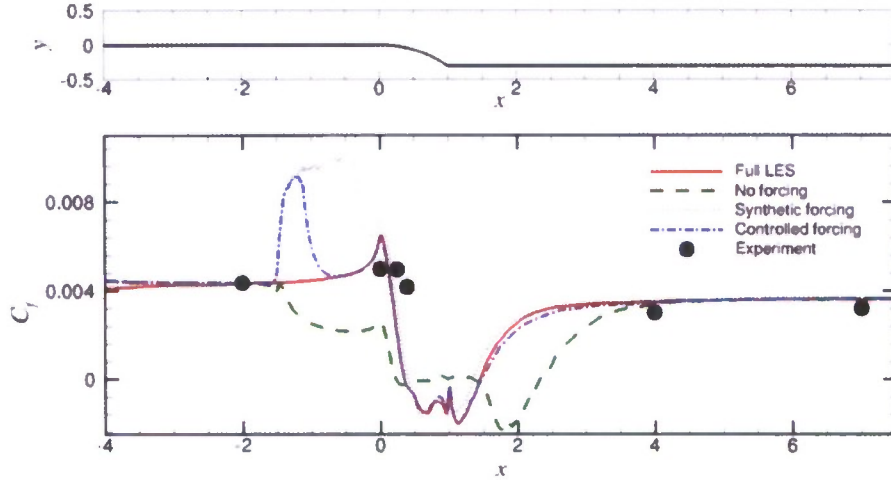
Figure 20: Skin-friction coefficient.

The skin-friction coefficient

$$C_f = \frac{\tau_w}{\rho U_R^2/2} \tag{28}$$

(where U_R is the average velocity at the reference location $x_R = -2$) is shown in Figure 20. The sudden decrease of the C_f at the RANS/LES interface in the calculation with no forcing is due to the fact that changing the length-scale in the Spalart-Allmaras model decreases the eddy viscosity. Since no eddies are present in this region (Figure 18), the turbulent wall-normal momentum transfer is effectively decreased, leading to a more laminar-like profile with decreased wall stress. The lower momentum of the fluid near the wall results in an early separation, and in a much more extended separation bubble. When the synthetic turbulence is used, we observe a significant increase of the skin friction in the region where the equations are manipulated (which is, of course, expected to be unphysical), but a recovery to the reference LES values shortly after the interface ends. Best results are obtained when the synthetic turbulence is coupled with the controlled forcing: the extent of the unphysical interface region was reduced, and very good agreement was achieved with the reference LES.

The profiles of the mean streamwise velocity and Reynolds shear stress are shown in Figure 21. When no forcing is used, the lack of momentum-supporting eddies discussed above results in vanishing resolved shear stress, which are not compensated by the modeled ones, Figure 21(b). The decreased momentum transport results in a more laminar-like velocity profile, which separates early. We have already commented on the effect of the early separation and the decreased mixing on the shape of the separation region when no forcing is used. Note that even at $x = 2$ the calculations with no forcing at the interface do not agree with the full simulations (the simulation predicts that the flow is still separated there), and only around $x = 4$, a considerable distance downstream of the ramp the mean velocity and Reynolds stresses agree with the full LES (the boundary layer thickness upstream of the ramp is $\delta_{\mathrm{ref}} = 0.33$).

4.4   Conclusions

This work showed the feasibility and utility of the use of forcing at the RANS/LES interface in actual single-block hybrid calculations of flows with shallow separation. When no special treatment is used at the RANS/LES interface, the behavior of the flow after the RANS/LES interface is incorrect. Lack of resolved eddies results in a decrease of the skin friction, which indicates a less full velocity profile near the wall, leading to early separation and to a recirculation bubble that is excessively long and high. Only a significant distance downstream (approximately 15 reference boundary layer thicknesses) the flow relaxes to its correct state.

When forcing is introduced immediately downstream of the RANS/LES interface, on the other hand, momentum-transporting eddies are generated more effectively, the prediction of the velocity profile is more
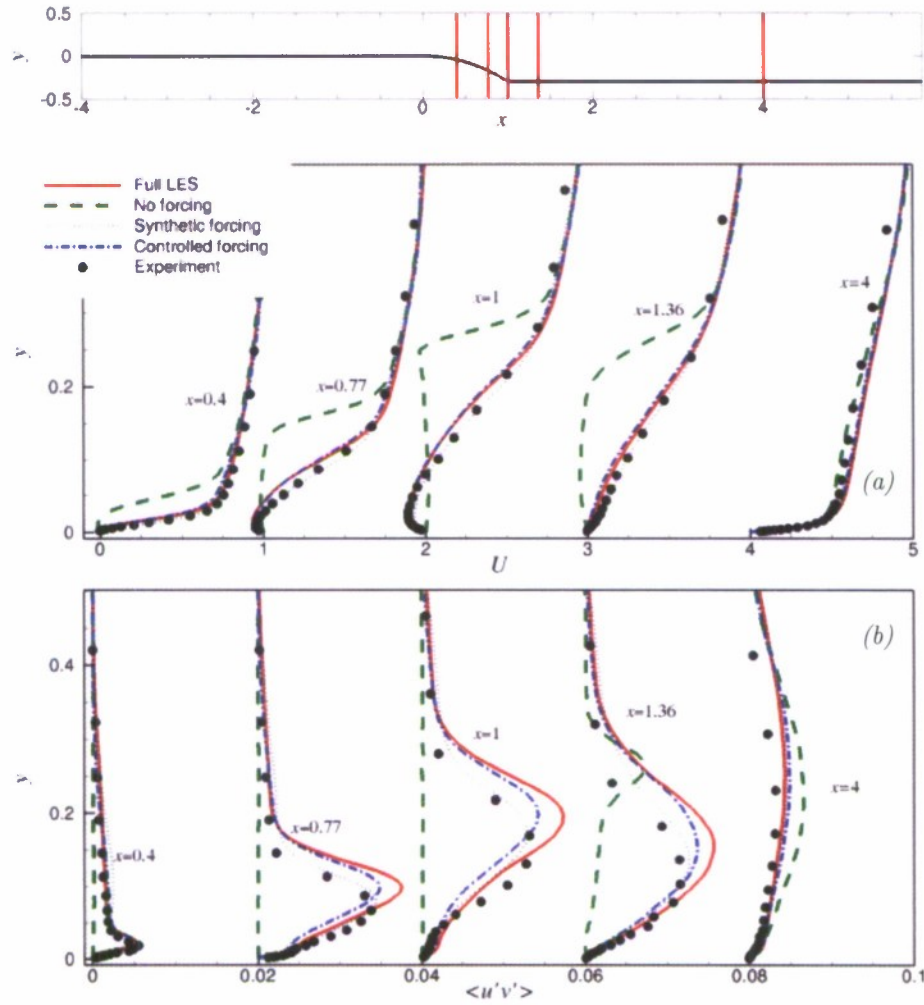
24

Figure 21: *(a)* Velocity profiles; *(b)* Reynolds shear stress profiles.

accurate, and the separation point (and, hence, the behavior of the flow downstream) is predicted well.

The controlled forcing was particularly effective in reducing the extent of the region in which the Navier-Stokes equations had to be manipulated. The comparison with the full LES and with the experimental data was quite good.

5 Summary

We have demonstrated the applicability of synthetic turbulence coupled with the controlled-forcing method to generate eddies at the interface between RANS and LES in hybrid calculations. By investigating the effects of the model parameter, and developing guidelines to set their values, we obtained shorter transition regions and improved model accuracy. It was found that realistic turbulence (with the correct statistics) can be generated within 5 boundary-layer thicknesses of the RANS/LES interface even in cases (such as the accelerating boundary layer) in which the data supplied by the RANS is inaccurate, or the assumptions on which the forcing is based are invalid.

We applied this technique in a variety of turbulent flows including phenomena such as freestream acceleration, separation, and mean flow three-dimensionality, with uniformly good results. A single-block hybrid calculation was then performed in a geometry that, although simple, presented several difficulties: because of the shallow pressure-driven separation, incorrect prediction of the upstream flow results in significant errors that propagate downstream, as the shear layer instability acts as an error amplifier. We demonstrated that unless turbulent eddies are artificially generated at the RANS/LES interface, very significant errors appear in the flow statistics even at low order (skin-friction coefficient, mean velocity profile). Establishing realistic turbulent eddies capable to transport momentum, energy and mass, appears to be a critical factor for the accurate prediction of shallow separation by hybrid RANS/LES methods.

Future work should concentrate on the application of this method in compressible boundary layers. In such cases the energy introduced by the forcing may be turned into internal energy, and be less effective at generating turbulent eddies, compared with incompressible cases. The generation of spurious pressure waves could also become an issue. This work will be proposed for a follow-up grant.

6 Personnel

The following personnel was supported on this grant:

1. U. Piomelli, Professor and PI.

2. E. Balaras, Assistant Professor and co-PI.

3. G. De Prisco, PhD student (Graduated Spring 2007).

4. S. Radhakrishnan, Postdoctoral Fellow.

7 Publications

The following publications that acknowledge AFOSR funding have appeared or have been accepted for publication:

1. G. De Prisco, A. Keating, and U. Piomelli. Large-eddy simulation of accelerating boundary layers. *AIAA Paper 2007-0725*, 2007.

2. G. De Prisco, A. Keating, U. Piomelli, and E. Balaras. Large-eddy simulation of accelerating boundary layers. In M. Oberlack, G. Khujadze, S. Guenther, T. Weller, M. Frewer, J. Peinke, and S. Barth, editors, *Progress in Turbulence II*, pages 137–144, Berlin, 2007. Springer-Verlag.

3. G. De Prisco, U. Piomelli, and A. Keating. Improved turbulence generation techniques for hybrid RANS/LES calculations. *J. Turbul.*, 9(5):1–20, 2008.

4. U. Piomelli, S. Radhakrishnan, and G. De Prisco. Turbulent eddies in the RANS/LES transition region. In S.-H. Peng and W. Haase, editors, *Advances in Hybrid RANS-LES Modelling*, volume 97 of *Notes on Numerical Fluid Mechanics and Multidisciplinary Design*, pages 21–36, Berlin, 2008. Springer-Verlag.

Note that the first two publications appeared during the present grant cycle but reported work performed under the previous grant cycle. One additional publication, on the hybrid calculations discussed in Section 4, is in preparation.

8 Interactions/Transitions

The research described in this report has been presented at the following seminars and conferences:

1. *59th Meeting of the Division of Fluid Mechanics of the American Physical Society*, Tampa, Florida, November 2006.

2. *45th AIAA Aerospace Sciences Meeting and Exhibit*, Reno, Nevada, January 2007.

3. *Second Symposium on Hybrid RANS-LES Methods*, Dassia, Greece, June 2007.

4. *61th Meeting of the Division of Fluid Mechanics of the American Physical Society*, San Antonio, Texas, November 2008.

5. Department of Mechanical and Aerospace Engineering, University of California, San Diego (CA), September 2007.

6. Department of Mechanical and Aerospace Engineering, Cornell University, Ithaca (NY), February 2009.

7. Department of Mechanical and Industrial Engineering, University of Toronto, Toronto (Ontario), Canada, March 2009.

References

[1] P. Batten, U. Goldberg, and S. Chakravarthy. Interfacing statistical turbulence closures with large-eddy simulation. *AIAA J.*, 42:485–492, 2004.

[2] P. Bradshaw, D. A. Ferriss, and N. P. Atwell. Calculation of boundary layer development using the turbulent energy equation. *J. Fluid Mech.*, 28:83–110, 1967.

[3] L. Davidson. Hybrid LES-RANS: Inlet Boundary Conditions. In B. Skallerud and H. Andersson, editors, *3rd National Conference on Computational Mechanics – MekIT'05*, pages 7–22, 2005.

[4] G. De Prisco, A. Keating, and U. Piomelli. Large-eddy simulation of accelerating boundary layers. *AIAA Paper 2007-0725*, 2007.

[5] M. Germano, U. Piomelli, P. Moin, and W. Cabot. A dynamic subgrid-scale eddy viscosity model. *Phys. Fluids A*, 3:1760–1765, 1991.

[6] A. Keating, G. De Prisco, and U. Piomelli. Interface conditions for hybrid RANS/LES calculations. *Int. J. Heat Fluid Flow*, 27:777–788, 2006.

[7] A. Keating, G. De Prisco, U. Piomelli, and E. Balaras. Interface conditions for hybrid RANS/LES simulations. In W. Rodi and M. Mulas, editors, *Engineering Turbulence Modeling and Experiments 6*, pages 349–358. Elsevier, 2005.

[8] A. Keating and U. Piomelli. A dynamic stochastic forcing method as a wall-layer model for large-eddy simulation. *J. Turbul.*, 7(12):1–24, 2006.

[9] A. Keating, U. Piomelli, E. Balaras, and H.-J. Kaltenbach. A priori and a posteriori tests of inflow conditions for large-eddy simulation. *Phys. Fluids*, 16(12):4696–4712, 2004.

[10] J. Kim and P. Moin. Application of a fractional step method to incompressible Navier-Stokes equations. *J. Comput. Phys.*, 59:308–323, 1985.

[11] M. Klein, A. Sadkiki, and J. Janicka. A digital filter based generation of inflow data for spatially developing direct numerical or large eddy simulations. *J. Comput. Phys.*, 186:652–665, 2003.

[12] H. Le, P. Moin, and J. Kim. Direct numerical simulation of turbulent flow over a backward-facing step. *J. Fluid Mech.*, 330:349–374, 1997.

[13] S. Lee, S. K. Lele, and P. Moin. Simulation of spatially evolving compressible turbulence and application of Taylor's hypothesis. *Phys. Fluids A*, 4:1521–1530, 1992.

[14] D. K. Lilly. The representation of small scale turbulence in numerical simulation experiments. In *Proccedings of the IBM Scientific Computing Symposium on Environmental Sciences*, pages 195–210, 1967.

[15] T. S. Lund, X. Wu, and K. D. Squires. Generation of inflow data for spatially-developing boundary layer simulations. *J. Comput. Phys.*, 140:233–258, 1998.

[16] F. Mathey, D. Cokljat, J.-P. Bertoglio, and E. Sergent. Assessment of the vortex method for large-eddy simulation inlet conditions. *Prog. Comput. Fluid Dyn.*, 6:59–67, 2006.

[17] C. Meneveau, T. S. Lund, and W. H. Cabot. A Lagrangian dynamic subgrid-scale model of turbulence. *J. Fluid Mech.*, 319:353–385, 1996.

[18] F. R. Menter. Eddy viscosity transport equations and their relation to the $k - \epsilon$ model. *ASME J. Fluids Eng.*, 119:876—884, 1997.

[19] Y. Na and P. Moin. Direct numerical simulation of a separated turbulent boundary layer. *J. Fluid Mech.*, 370:175–201, 1998.

[20] N. V. Nikitin, F. Nicoud, B. Wasistho, K. D. Squires, and P. R. Spalart. An approach to wall modeling in large-eddy simulations. *Phys. Fluids*, 12:1629–1632, 2000.

[21] I. Orlanski. A simple boundary condition for unbounded hyperbolic flows. *J. Comput. Phys.*, 21:251–269, 1976.

[22] U. Piomelli and E. Balaras. Wall-layer models for large-eddy simulations. *Annu. Rev. Fluid Mech.*, 34:349–374, 2002.

[23] S. Radhakrishnan, U. Piomelli, and A. Keating. Wall-modeled large-eddy simulations of flows with curvature and mild separation. *ASME J. Fluids Eng.*, 130:101203-1–8, 2008.

[24] S. Radhakrishnan, U. Piomelli, A. Keating, and A. Silva Lopes. Reynolds-averaged and large-eddy simulations of turbulent non-equilibrium flows. *J. Turbul.*, 7(63):1–30, 2006.

[25] C. Rhie and W. Chow. Numerical study of the turbulent flow past an airfoil with trailing edge separation. *AIAA J.*, 21:1525–1532, 1983.

[26] N. Sandham, Y. Yao, and A. Lawal. Large-eddy simulation of transonic turbulent flow over a bump. *Int. J. Heat Fluid Flow*, 24:584–595, 2004.

[27] J. Schlüter, H. Pitsch, and P. Moin. LES inflow conditions for coupling with Reynolds-averaged flow solvers. *AIAA J.*, 42:478–484, 2004.

[28] J. U. Schlüter, X. Wu, S. Kim, J. J. Alonso, and H. Pitsch. Coupled RANS-LES computation of a compressor and combustor in a gas turbine engine. *AIAA Paper 2004-3417*, 2004.

[29] A. Silva Lopes and J. M. L. M. Palma. Simulations of isotropic turbulence using a non-orthogonal grid system. *J. Comput. Phys.*, 175(2):713–738, 2002.

[30] A. Silva Lopes, U. Piomelli, and J. M. L. M. Palma. Large-eddy simulation of the flow in an S-duct. *J. Turbul.*, 7(11):1–24, 2006.

[31] J. Smagorinsky. General circulation experiments with the primitive equations. I. The basic experiment. *Mon. Weather Rev.*, 91:99–164, 1963.

[32] A. Smirnov, S. Shi, and I. Celik. Random flow generation technique for large eddy simulations and particle-dynamics modeling. *ASME J. Fluids Eng.*, 123:359–371, 2001.

[33] S. Song and J. K. Eaton. Reynolds number effects on a turbulent boundary layer with separation, reattachment, and recovery. *Exp. Fluids*, 36:246–258, 2004.

[34] P. Spalart and S. Allmaras. A one-equation turbulence model for aerodynamic flows. *La Recherche Aérospatiale*, 1:5–21, 1994.

[35] P. Spalart, S. Deck, M. Shur, K. D. Squires, M. K. Strelets, and A. Travin. A new version of detached-eddy simulation, resistant to ambiguous grid densities. *Theor. Comput. Fluid Dyn.*, 20:181–195, 2006.

[36] P. R. Spalart. Strategies for turbulence modelling and simulations. *Int. J. Heat Fluid Flow*, 21:252–263, 2000.

[37] P. R. Spalart. Detached-eddy simulation. *Annu. Rev. Fluid Mech.*, 41:181–202, 2009.

[38] P. R. Spalart, W. H. Jou, M. K. Strelets, and S. R. Allmaras. Comments on the feasibility of LES for wings, and on a hybrid RANS/LES approach. In C. Liu and Z. Liu, editors, *Advances in DNS/LES*, pages 137–148, Columbus, OH, 1997. Greyden Press.

[39] A. Spille-Kohoff and H.-J. Kaltenbach. Generation of turbulent inflow data with a prescribed shear-stress profile. In C. Liu, L. Sakell, and T. Beutner, editors, *DNS/LES Progress and challenges*, pages 319–326, Columbus, OH, 2001. Greyden Press.

[40] M. Terracol. A zonal RANS/LES approach for noise sources prediction. In W. Rodi and M. Mulas, editors, *Engineering Turbulence Modelling and Experiments 6*, pages 699–708, Amsterdam, 2005. Elsevier.

[41] D. Warnack and H. H. Fernholz. The effects of a favourable pressure gradient and of the reynolds number on an incompressible axisymmetric turbulent boundary layer. part 2. the boundary layer with relaminarization. *J. Fluid Mech.*, 359:357–371, 1998.